The University of British Columbia

FACULTY OF GRADUATE STUDIES

PROGRAMME OF THE

FINAL ORAL EXAMINATION

FOR THE DEGREE OF

DOCTOR OF PHILOSOPHY

of

JAMES WHITTEKER

B.Sc. Carleton University, 1962

FRIDAY, OCTOBER 6, 1967, AT 3:30 P.M.

ROOM 301, HENNINGS BUILDING

COMMITTEE IN CHARGE

Chairman: B. N. Moyls

F.W. Dalby	M. McMillan
B. Ahlborn	H. Gush
C.E. Brion	C.A. McDowell

External Examiner: Prof. Robert Krotkov
University of Massachusetts
Amherst Massachusetts

Research Supervisor: F.W. Dalby

POLARIZATION OF ELECTRON IMPACT LIGHT FROM HELIUM

ABSTRACT

The polarization of light from helium atoms excited by the impact of low energy electrons has been measured for the spectral lines $2^3P - 2^3S$ (10,829 Å) and $3^3P - 2^3S$ (3889 Å). An electron beam carrying a current of 10 μA was directed into helium gas at a pressure of 4×10^{-3} torr or less. Polarization was measured as a function of electron energy in a range from the excitation threshold (approximately 23 electron volts) to 50 e.v. For the $2^3P - 2^3S$ line, this work represents the first reported measurement of this type.

There is special interest in the value of polarization near the excitation threshold. The theoretical threshold polarization for both lines studied in this thesis is 36.6%. In the experiment of this thesis, the observed polarization of the 2^3P line rises to 21% near threshold, and by means of a curve fitting procedure may be extrapolated to $32 \pm 6\%$. The polarization of the $3^3P - 2^3S$ line rises to 11% and may be extrapolated to $15 \pm 3\%$.

GRADUATE STUDIES

Field of Study: Atomic Physics

Elementary Quantum Mechanics	W. Opechowski
Waves	J.C. Savage
Electromagnetic Theory	G.M. Volkoff
Nuclear Physics	J.B. Warren
Plasma Physics	L. de Sobrino
Spectroscopy	A.M. Crooker
Special Relativity Theory	H. Schmidt
Molecular Spectroscopy	F.W. Dalby
Advanced Spectroscopy	A.J. Barnard
Advanced Quantum Mechanics	H. Schmidt

AWARDS

1958-61	International Nickel Co. Scholarship
1962-65	National Research Council Scholarship
1966	UBC Graduate Fellowship
1967	National Research Council Postdoctorate Fellowship

POLARIZATION OF ELECTRON IMPACT LIGHT FROM HELIUM

by

JAMES HOWARD WHITTEKER

B.Sc., Carleton University, 1962

A THESIS SUBMITTED IN PARTIAL FULFILMENT OF

THE REQUIREMENTS FOR THE DEGREE OF

DOCTOR OF PHILOSOPHY

in the Department

of

PHYSICS

We accept this thesis as conforming to the

required standard

THE UNIVERSITY OF BRITISH COLUMBIA

October, 1967

In presenting this thesis in partial fulfilment of the requirements for an advanced degree at the University of British Columbia, I agree that the Library shall make it freely available for reference and Study. I further agree that permission for extensive copying of this thesis for scholarly purposes may be granted by the Head of my Department or by his representatives. It is understood that copying or publication of this thesis for financial gain shall not be allowed without my written permission.

Department of Physics

The University of British Columbia
Vancouver 8, Canada

Date Oct. 6, 1967

ABSTRACT

The polarization of light from helium atoms excited by the impact of low energy electrons has been measured for the spectral lines $2^3P - 2^3S$ (10,829 Å) and $3^3P - 2^3S$ (3889 Å). An electron beam carrying a current of 10μA was directed into helium gas at a pressure of 4×10^{-3} torr or less. Polarization was measured as a function of electron energy in a range from the excitation threshold (approximately 23 electron volts) to 50 e.v. For the $2^3P - 2^3S$ line, this work represents the first reported measurement of this type.

There is special interest in the value of polarization near the excitation threshold. The theoretical threshold polarization for both lines studied in this thesis is 36.6%. In the experiment of this thesis, the observed polarization of the 2^3P line rises to 21% near threshold, and by means of a curve fitting procedure may be extrapolated to 32 ± 6%. The polarization of the $3^3P - 2^3S$ line rises to 11% and may be extrapolated to 15 ± 3%.

TABLE OF CONTENTS

LIST OF TABLES

LIST OF FIGURES

ACKNOWLEDGEMENTS

I wish to thank Professor F. W. Dalby for suggesting the problem and for supervising the research.

I wish also to thank my wife for her valuable assistance in the preparation of this thesis.

This work was supported by The National Research Council of Canada.

CHAPTER I

INTRODUCTION

Atomic line radiation excited by electron impact will, in general, be polarized relative to an axis parallel to the electron beam. A simple way to visualize the effect is to think of the atom as a collection of charged particles connected by springs. If this atom is hit directly by a projectile travelling in the z direction, the atom will tend to vibrate in modes in which the displacements of the electric charges are along the z axis. The light that is radiated, then, will be polarized to some extent along the z axis. It turns out that the polarization observed is, in fact, usually positive with respect to the z axis, as one would expect from the description just given, although a minority of spectral lines show negative polarization.

When we wish to speak quantitatively of the polarization, we use the following definition for the degree of polarization P. If $I^{\parallel}$ is the intensity of light with its electric vector in the direction of the electron beam, and if $I^{\perp}$ is the intensity of light with its electric vector in the direction perpendicular to the electron beam, we have

$$P = \frac{I^{\parallel} - I^{\perp}}{I^{\parallel} - I^{\perp}}$$

It is usually understood that the light is viewed from a direction perpendicular to the electron beam.

It is very difficult to make detailed predictions of the polarization of light due to electron impact. For a given spectral line, the polarization depends in general on the details of the collision process, and is therefore difficult to calculate. Even though the laws governing electron-atom collisions at non-relativistic energies are completely known, the calculation of low energy scattering and excitation cross sections at low energies is extremely complex. By low energies is meant energies less than a few hundred electron volts, in the region where the Born approximation does not apply. In fact, even though there has been intensive work on electron-atom scattering in the past few years the only type of electron-atom scattering that can be calculated accurately is electron-hydrogen elastic scattering,[1] and to a lesser extent, electron-hydrogen inelastic scattering.[2] For other cases, one can make approximations, such as the distorted wave approximation, that are somewhat better at low energies than the Born approximation, but which cannot really be expected to produce detailed, accurate cross sections.[1] This implies that they also cannot be expected to produce detailed, accurate polarization curves.

In spite of these difficulties, it is possible to make a unique prediction for the polarization of a given line very close to the excitation threshold for that line. This prediction

depends only on angular momentum considerations, as will be seen in Chapter II. The polarization predicted at threshold is the maximum possible for that spectral line.

Measurements of the polarization of light due to electron impact were made for a number of atoms by several workers during the years 1925 to 1935.[3] During the same period a number of measurements were made of a related phenomenon, the polarization of light due to the absorbtion of resonance radiation.[4] Of the electron impact experiments, the only ones that involved a detailed study of the polarization as a function of the energy of the electrons were those by Skinner and Appleyard.[5] They studied several lines in the mercury spectrum, and measured the polarization of light due to electrons ranging in energy from 0.5 or 1 e.v. above threshold to about 200 e.v. Typically their curves have the general appearance of the one shown in Figure 1(B). With decreasing electron energy, the polarization rises in magnitude to a maximum which occurs a few volts above threshold. Then as threshold is approached more closely, the polarization drops toward zero. This last effect is one that is contrary to theoretical expectations, which indicate a curve of the form shown in Figure 1(A).

In the past few years, there has been a revival of interest in the subject due to the use of polarization measurements as a means of detecting microwave transitions.[6] Most of the recent measurements, however, have not been concerned with polarization

as a tool for other experiments, but have been done with a view to understanding the phenomena involved. This is true also of the measurements described in this thesis. In the past few years there have been polarization measurements on atomic hydrogen, helium II, lithium, sodium, and mercury.[7]

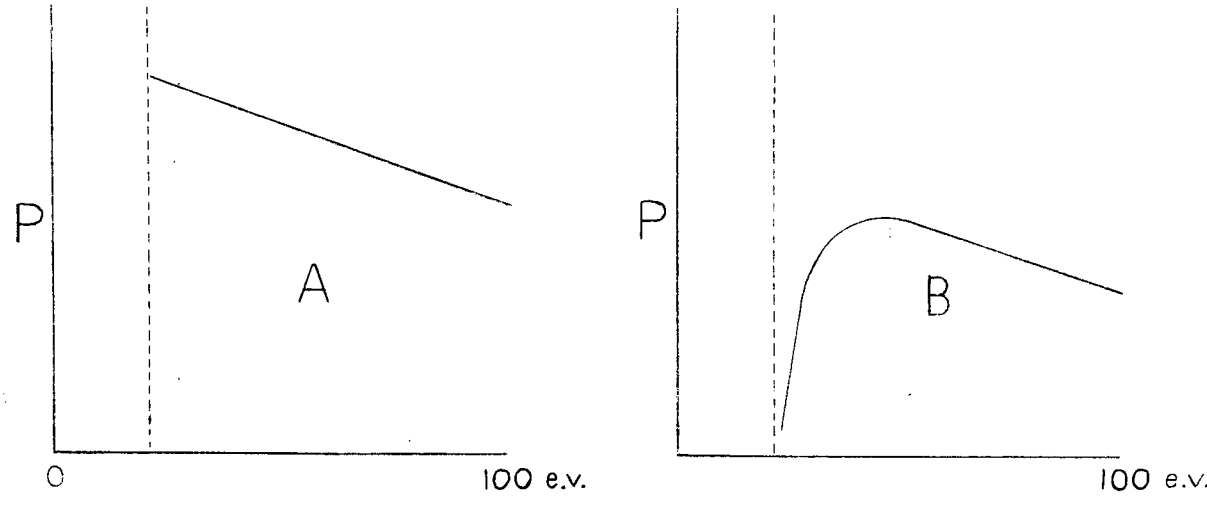

Fig. 1. Expected (A) and observed (B) polarization curves.

The results of these experiments may be described briefly as follows:

H: Measurements indicate that the polarization remains finite near threshold, but do not allow a comparison of the threshold value with theory. This is because the Balmer α data involve three unresolved lines with unknown intensity ratios, and because the Lyman α results are very imprecise.

He: The polarization of most of the lines varies rapidly near threshold. Curves of the form of Figure 1(B) are common in the work before 1963, but do not appear in results published since then, and it appears that the effect is a property of the experimental method rather than a property of electron-helium collisions. Nevertheless, except in the case of some of the most recent work,[8] the polarization has not been observed to come close to the theoretical value at threshold. In the case of the exception just mentioned, the polarization is observed to rise to the threshold value from a minimum that is very close to threshold.

He II: The polarization of one line has been shown to increase monotonically with decreasing electron energy, but comparison with theory is impossible.

Li^6, Li^7, Na^{23}: The polarizations of the resonance lines have been found to rise monotonically with decreasing electron energy (as in curve A) and to approach the predicted value at threshold, exactly as one would expect. In fact these measurements are good enough to check the previously published values of hyperfine structure and natural line width. However, there is a lithium line for which the polarization decreases close to threshold.

Hg: The polarization of the D lines is finite near threshold, but the observations involve two unresolved lines with an unknown intensity ratio. These results indicate,

however, that the earlier results of Skinner and Appleyard were wrong near threshold, probably as a result of the low light intensities involved.

The question to be answered then, is that of the behavior of the polarization curves near threshold. This is where theory gives a definite answer, and this is also where measurements are difficult because intensities are low. The experimental work described in this thesis pursues that question for two lines in the helium spectrum.

The energy level diagram for helium is shown in Figure 2. The lines connecting different energy levels represent spectral lines or multiplets for which the polarization due to electron impact has been measured. Double lines indicate those for which data appear in this thesis. The numbers at the top of the columns indicate the theoretical threshold polarizations from lines (in the case of singlet levels) or multiplets (in the case of triplet levels) originating in these columns. These numbers apply to $L \rightarrow L - 1$ transitions in the case of upper P and D states, and $L \rightarrow L + 1$ transitions in the case of upper S states.

The largest polarizations have been observed with ^1D-^1P lines. The ^1P-^1S lines are predicted to have the largest polarizations, but the observed polarizations are not high, probably because, except at very low pressures, some of the light is due to excitation by trapped resonance radiation. The 3^3P-2^3S

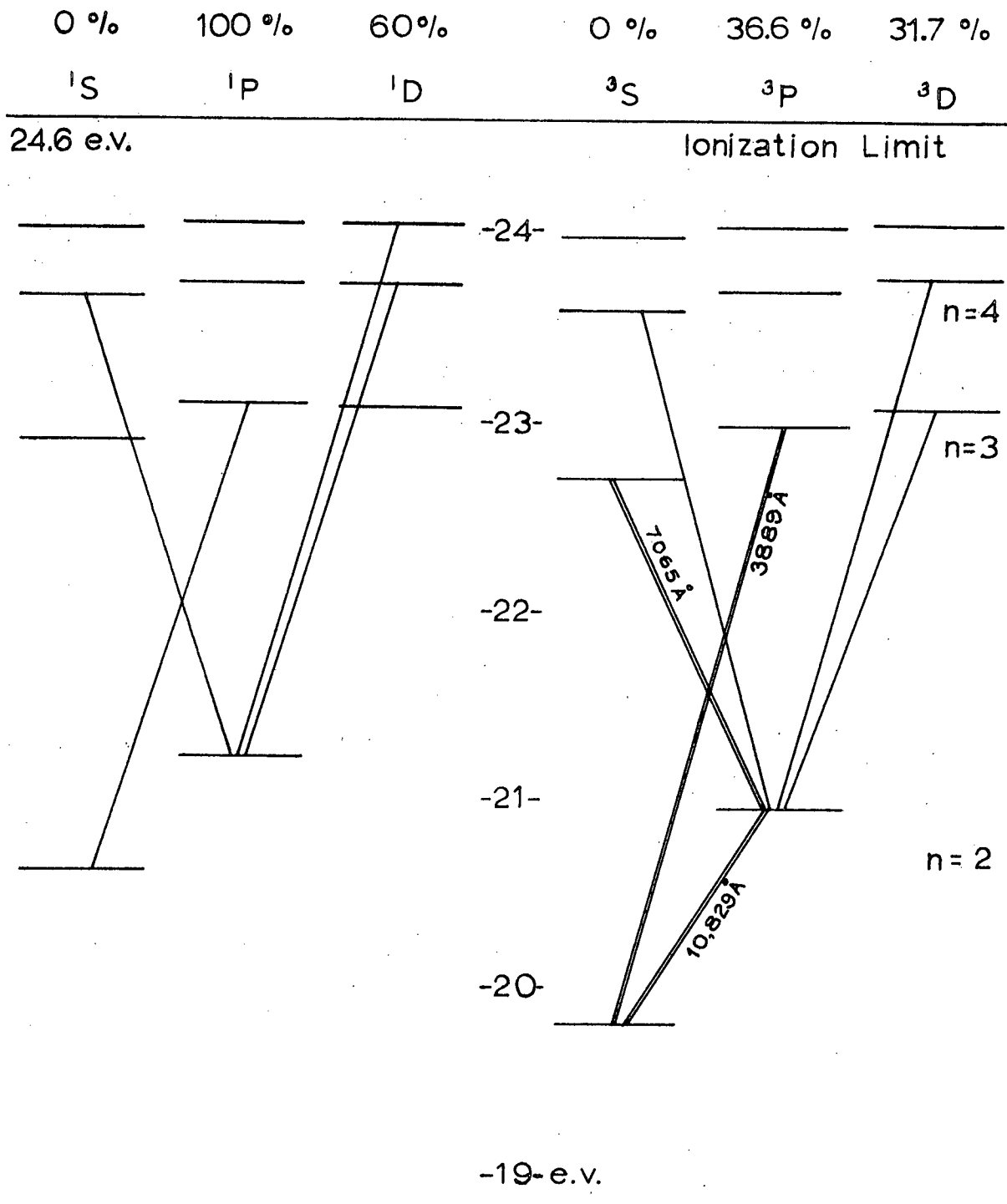

Fig. 2. Energy Level Diagram for Helium. The ground state, which is not shown, is a ^1S state and is at zero electron volts.

(3889Å) transition is the only one for which the polarization did not, until recently, appear to approach zero near threshold.

The primary concern of this thesis is the polarization of the 2^3P-2^3S (10,829Å) multiplet of helium. This multiplet is of particular interest because it originates from a low lying level that is comparatively well separated from neighbouring levels, and because some theoretical work has been done on it. Until now, no optical measurements of polarization have been reported for this multiplet, although the alignment of the 2^3S level resulting from the 2^3P-2^3S transition has been measured by an atomic beam method.[9]

The 3^3P-2^3S (3889Å) multiplet is also studied in this thesis. In this case, the work is not new, although the statistical accuracy is somewhat higher than in previous measurements. Because other workers have studied this multiplet, the results presented here also serve as a test of the experimental method.

References and Footnotes for Chapter I

1. A brief and lucid account of the state of low energy electron-atom scattering theory as of 1964 is given by E. Gerjuoy in Physics Today 18, 24 (May 1965).

2. P. G. Burke, H. M. Schey, K. Smith, Phys. Rev. 129, 1258 (1963).

3. References for this early work are given by I. C. Percival and M. J. Seaton, Phil. Trans. Ser. A 251, 113 (1958).

4. An account of this work is given in A.C.G. Mitchell and M. W. Zemansky, Resonance Radiation and Excited Atoms (Cambridge University Press, London, 1961).

5. H.W.B. Skinner and E.T.S. Appleyard, Proc. Roy. Soc. (London) Ser. A 117, 224 (1927).

6. For example, W. E. Lamb and T. H. Maiman, Phys. Rev. 105, 573 (1957).

7. References for recent polarization measurements are listed below with respect to the atomic species studied.

H: H. Kleinpoppen, H. Kruger, and R. Ulmer, Physics Letters 2, 78 (1962).

W. L. Fite and R. T. Brackmann, Phys. Rev. 112, 1151 (1958).

He: R. H. McFarland and E. A. Soltysik, Phys. Rev. 127, 2090 (1962).

D. W. O. Heddle and C. B. Lucas, Proc. Roy. Soc. (London) Ser. A 271, 129 (1963).

R. H. Hughes, R. B. Kay, L. D. Weaver, Phys. Rev. 129, 1630 (1963).

(8). R. H. McFarland, Phys. Rev. Letters 10, 397 (1963).

(8). D.W.O. Heddle and R.G.W. Keesing, Proc. Roy. Soc. (London) Ser. A 258, 124 (1967).

E. A. Soltysik, A. Y. Fournier and R. L. Gray, Phys. Rev. 153, 152 (1967).

(8). R. H. McFarland, Phys. Rev. 156, 55 (1967).

Li^6, Li^7, Na^{23}:
H. Hafner and H. Kleinpoppen, Zeit. Phys. 198, 315 (1967).

Hg: H. G. Heideman, Physics Letters 13, 309 (1964).

9. H. K. Holt and R. Krotkov, Phys. Rev. 144, 82 (1966).

CHAPTER II

THEORY

2.1 Introduction

The theory of the polarization of light from atoms due to electron impact has been reviewed and developed by Percival and Seaton. They derive expressions for polarization in terms of the relative cross sections for excitation to the various M_L states, where M_L is the Z component of orbital angular momentum. They do not attempt to calculate the cross sections themselves. Such a calculation involves all the details of the collision process and at best can be done only approximately. However, at threshold, one can predict the polarization without a detailed knowledge of the collision process. This will be discussed later. The theory developed by Percival and Seaton is restricted to atoms which can be described in terms of LS coupling, and which have zero orbital angular momentum in their ground states, and it is also restricted to dipole radiation. Otherwise it is quite general. The effect of hyperfine structure is calculated, including the case in which the hyperfine separation is comparable with the natural line width. (This is of interest in the case of atomic hydrogen.)

In the following pages I shall outline the theory that is applicable to helium. Hyperfine structure will

therefore be ignored. The theory presented here will follow Percival and Seaton quite closely in discussing the collision process, but will depart from them to some extent in discussing the radiation process. Percival and Seaton use the tensor operator methods developed by Racah, while the theory presented here will use the more pedestrian methods described by Condon and Shortley.

The emission of radiation due to electron impact is considered to take place in two distinct steps:

(i) the collision process, in which the atom is excited from the initial (usually ground) state to an excited state β, and

(ii) the radiation process, in which the atom drops to state γ, with the emission of a photon. (See Figure 3)

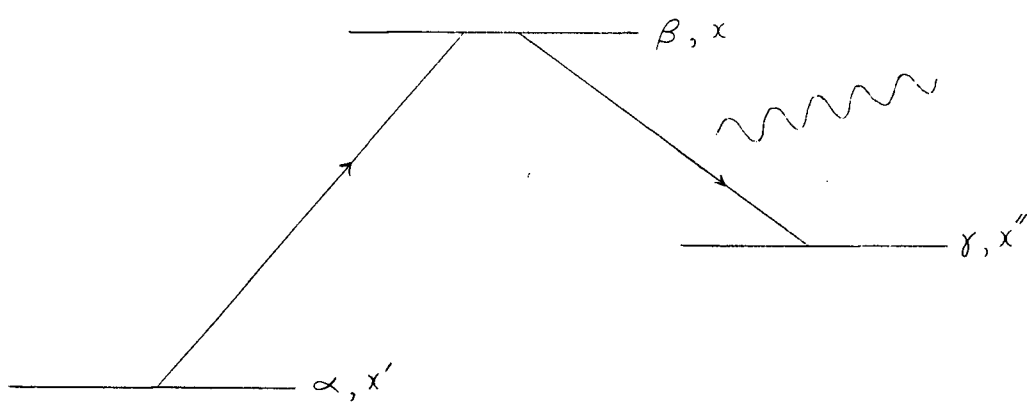

Fig. 3. Excitation and Emission.

These two processes take place on quite different time scales. The collision process takes a time presumably of the order of 10^{-14} sec. (the transit time of the scattered electron at 0.1 volts) or less (for higher energies). The radiation time is much longer, 10^{-7} sec. for the lines studied in this thesis. There is another time interval of importance, namely the time required to transfer angular momentum from the orbital state of an atom to its spin state, and vice versa.

As an estimate of this spin-orbit interaction time, we take the inverse of the fine structure transition angular frequency, i.e. $1/2\pi f$. The shortest interaction time found in this way for helium is 10^{-11} sec., which occurs in the 2^3P state. Thus, to a good approximation, we can consider that, for the duration of the collision process, the spin and orbital angular momenta are uncoupled. On similar grounds, we may assert that there is no spin-orbit interaction between the atom and the incident electrons. For the reasons given above, we can assume that spin and orbital angular momenta are separately conserved during the collision, and that spin coordinates are not involved in the collision process. Since spin is left out of the picture during the collision, the relevant quantities in a description of the collision process are the cross sections for excitation to the various orbital angular

momentum states. These states we label by their M_L values, and we denote the cross sections by Q_{M_L}.

In order to describe the radiation process, however, we must describe the excited states of the atom in the LS coupled scheme. We require, therefore, a relation between the excitation cross sections in the LS coupled scheme and the cross sections Q_{M_L} in the uncoupled scheme. This is what is done in the next section.

2.2 Collision Process

The wave function of the scattered electron at a large distance r from the scattering centre has the form $\frac{e^{ikr}}{r} f_\beta(\underline{k})$, where $f_\beta(\underline{k})$ is called the scattering amplitude, and is a function of the direction $(\underline{k})$. The subscript indicates the state into which the atom is excited. The cross section for scattering into a solid angle $d\omega$ about direction $(\underline{k})$ is proportional to $|f_\beta(\underline{k})|^2 d\omega$, and the total cross section for excitation into state β is proportional to $|f_\beta(\underline{k})|^2 d\omega$. Now the relationship between the scattering amplitudes in the $\beta = SLJM_J$ scheme and the $\beta = SLM_SM_L$ scheme is

$$f_{SLJM_J}(\underline{k}) = \sum_{M_S M_L} C^{S\ L\ J}_{M_S M_L M_J} f_{SLM_SM_L}(\underline{k}) \qquad (1)$$

where the $C^{S\ L\ J}_{M_S M_L M_J}$ are vector coupling coefficients. It follows that

$$\int |f_{SLJM_J}(\underline{k})|^2 d\omega =$$

$$\sum_{\substack{M_S M_L \\ M'_S M'_L}} C^{S\ L\ J}_{M_S M_L M_J} C^{S\ L\ J}_{M^\circ_S M^\circ_L M_J} \int f_{SLM_S M_L}(\underline{k}) f_{SLM^\circ_S M^\circ_L}(\underline{k}) d\omega \qquad (2)$$

We can eliminate the mixed terms in this expression by applying our assumption that spin and orbital angular momenta are separately conserved during the collision. These conditions are:

$$M_L + m_l = 0 \qquad (3)$$

$$M_S + m_S = M'_S - m'_S \qquad (4)$$

where m′ refers to the incident electron and m to the scattered electron. In the following discussion letters with a single prime refer to the initial level; unprimed letters refer to the excited level; and letters with a double prime refer to the level after radiation has taken place. Refer to Figure 3. The right hand side of (3) is zero because in the initial state, $M'_L=0$ by assumption. We have $m'_l=0$ because we define the z axis to be directed parallel to the direction of travel of the incident electron.

If we expand the scattering amplitude into spherical harmonics in the following way,

$$f_{SLM_S M_L}(\underline{k}) = \sum_{l m_l} Y_{lm}(\underline{k}) f(SLM_S M_L) \qquad (5)$$

we find, by applying the conservation conditions, that

$$\int f^*_{SLM_S M_L} f_{SLM^\circ_S M^\circ_L} d\omega$$

vanishes unless $M_S=M^\circ_S$, $M_L=M^\circ_L$.

Hence

$$\int |f_{SLJM_J}(\underline{k})|^2 = \sum_{M_S M_L} \left(C^{S\ L\ J}_{M_S M_L M_J}\right)^2 \int |f_{SLM_S M_L}(\underline{k})|^2 \, d\omega \tag{6}$$

Therefore the cross section is given by

$$Q_{SLJM_J} = \sum_{M_S M_L} \left(C^{S\ L\ J}_{M_S M_L M_J}\right)^2 Q_{SLM_S M_L} \tag{7}$$

Now by our previous assumption, $Q_{SLM_S M_L}$ is independent of M_S, so we write

$$Q_{M_L} = (2S+1)\, Q_{SLM_S M_L} \tag{8}$$

Furthermore, because of the axial symmetry of the system, Q_{M_L} is independent of the sign of M_L. That is, there is nothing in the system to favour left or right hadd rotations. Hence we write

$$Q_{M_L} = Q_{|M_L|} \tag{9}$$

This leaves us with

$$Q_{SLJM_J} = \sum_{M_S M_L} \left(C^{S\ L\ J}_{M_S M_L M_J}\right)^2 \frac{1}{2S+1}\, Q_{|M_L|} \tag{10}$$

which is the relationship we set out to find.

We shall also require the relative probabilities of exciting the various fine structure levels.

We have

$$Q_J = \sum_{M_J} Q_{SLJM_J} = \sum_{M_S M_L M_J} \left(C^{S\ L\ J}_{M_S M_L M_J}\right)^2 \frac{1}{2S+1}\, Q_{|M_L|} \tag{11}$$

But

$$\sum_{M_S M_J} \left(C^{S\ L\ J}_{M_S M_L M_J}\right)^2 = \frac{2J+1}{2L+1} \tag{12}$$

This follows from the symmetry properties of the vector coupling coefficients. Therefore

$$Q_J = \frac{2J+1}{(2L+1)(2S+1)} Q_{S_L} \tag{13}$$

where we define $Q_{S_L} = \sum_{M_L} Q_{|M_L|}$

As we might expect then, the cross section for exciting a given fine structure level is simply proportional to the statistical weight of that level.

2.3 The Radiation Process

Our next task is to find the polarization of the radiation that is due to each $JM_J \rightarrow J''M_J''$ transition. After that, we sum over M_J and M_J'' to obtain the polarization of each spectral line. Finally, we sum over J and J'' to obtain the polarization of the multiplet, which is the quantity that is measured.

The degree of polarization is defined as

$$P = \frac{I'' - I^{\perp}}{I'' + I^{\perp}} \tag{14}$$

We now put this into a form that is more convenient for calculations. Define

$$I_x = I_y = I_{\perp}, \qquad I_z = I'', \qquad \bar{I} = I_x + I_y + I_z$$

Then we obtain

$$P = \frac{3I_z - \bar{I}}{I_z + \bar{I}} \tag{15}$$

The polarization, then, is determined by the relative values of I_Z and I, and this is what we now calculate. The emission rate A^{μ} for light of a given polarization μ in the transition

$JM_J \rightarrow J'' M_J''$ is proportional to the square of the transition moment. That is, we have

$$A(JM_J \rightarrow J''M_J'') = K|\langle J M_J | P_\mu | J'' M_J'' \rangle|^2 \qquad (16)$$

where $\underline{P}$ is the dipole moment operator

$$P_0 = P_z$$
$$P_{\pm 1} = \frac{P_x \pm i P_y}{\sqrt{2}}$$

K is a constant characteristic of the multiplet. The M_J, M_J'' dependence of (16) is given by Condon and Shortley, The Theory of Atomic Spectra, (which will be referred to as TAS) equations $9^3 11$. Bearing in mind the required quantities in (15), and noticing that this is a convenient point at which to sum over M_J'', we obtain

$$A^\circ(JM_J \rightarrow J'') = K|\langle JM_J | P_0 | J'' M_J \rangle|^2$$
$$A(JM_J \rightarrow J'') = K \sum_{\mu M_J''} |\langle J M_J | P_\mu | J'' M_J'' \rangle|^2 = K|\langle J | P | J'' \rangle|^2 \Xi(J, J'') \qquad (17)$$

where the $\langle J \| P \| J'' \rangle$ are the reduced matrix elements of TAS $9^3 11$, and the $\Xi(J, J)$ are the result of summing the $M_J M_J''$ dependent part of the matrix elements over μ. They are

$$\Xi(J, J+1) = (J+1)(2J+3)$$
$$\Xi(J, J) = J(J+1) \qquad (18)$$
$$\Xi(J, J-1) = J(2J-1) \qquad \text{(TAS } 7^4 5\text{)}$$

Equations (17) give the rate of emission in the $(J \rightarrow J'')$ line from one atom in the state JM_J. The rate of excitation of

atoms to the state JM_J is proportional to the excitation cross section to that state, which is

$$Q_{JM_J} = \sum_{M_S M_L} \left(C^{S\ L\ J}_{M_S M_L M_J}\right)^2 \frac{1}{2S+1} Q_{|M_L|} \tag{10}$$

The rate of radiation is proportional to the quantities

$$Q_{JM_J} \frac{A^0(JM_J \to J'')}{A(SLJM_J)} =$$

$$\frac{K}{A(SLJM_J)} \sum_{M_J M_L} \left(C^{S\ L\ J}_{M_S M_L M_J}\right)^2 \frac{1}{2S+1} Q_{|M_L|} \left|\langle JM_J | P_0 | J'' M_J \rangle\right|^2$$

$$Q_{JM_J} \frac{A(JM_J \to J'')}{A(SLJM_J)} =$$

$$\frac{K}{A(SLJM_J)} \sum_{M_S M_L} \left(C^{S\ L\ J}_{M_S M_L M_J}\right)^2 \frac{1}{2S+1} Q_{|M_L|} \left|\langle J | P | J'' \rangle\right|^2 \Xi(J, J'') \tag{19}$$

where $A(SLJM_J)$ is the total emission rate from the state $SLJM_J$.

Next, to find the rates of emission in the spectral line $J \longrightarrow J''$, we sum (19) over M_J to obtain

$$I^2(J \to J'') = \frac{K^0}{2S+1} \sum_{M_S M_L M_J} \left(C^{L\ S\ J}_{M_L M_S M_J}\right)^2 Q_{|M_L|} \left|\langle JM_J | P_0 | J'' M_J \rangle\right|^2$$

$$\bar{I}(J \to J'') = K^0 \frac{2J+1}{(2L+1)(2S+1)} \sum_{M_L} Q_{|M_L|} \left|\langle J | P | J'' \rangle\right|^2 \Xi(J, J'') \tag{20}$$

where we have used (12) and (13). K has been replaced by K^0 in order to accommodate such quantities as atom density and electron beam current, and $A(SLJM_J)$ which is independent of J and M_S (TAS $13^3 5$).

Equations (20) enable us to derive expressions for the polarization of light in a given spectral line by use of

equation (15). We require the M_J dependence of $\langle JM_J | P_0 | J'' M_J \rangle$ which is given in TAS $9^3 11$ and the vector coupling coefficients tabulated in TAS p. 76.

In the case of helium singlet lines, the procedure is quite easy, since the vector coupling coefficients reduce to unity, and we have $J = L$, $J'' = L''$. In the case of helium triplet lines, however, there is even more work to do, because we want the polarization of the whole multiplet. After summing equations (20) over M_J, we must then sum over J and J''. This can be done using the expressions for the J and J'' dependence of $\langle J | P | J'' \rangle$ given in TAS $11^3 8$.

The results of these calculations appear in the following form:

For upper S states (L=0)

$$P = 0 \tag{21}$$

For $P \rightarrow S$ $(L = 1 \rightarrow L = 0)$ lines or multiplets

$$P = \frac{G(Q_0 - Q_1)}{h_0 Q_0 + h_1 Q_1} \tag{22}$$

For $D \rightarrow P$ $(L = 2 \rightarrow L = 1)$ lines or multiplets

$$P = \frac{G(Q_0 + Q_1 - 2Q_2)}{h_0 Q_0 + h_1 Q_1 + h_2 Q_2} \tag{23}$$

These formulae and numerical tables of the coefficients are given in Percival and Seaton, Tables 1 and 2. In the case of ^3P-^3S multiplets (the ones studied in the thesis) we have

$$P = \frac{15(Q_0 - Q_1)}{41 Q_0 + 67 Q_1} \tag{24}$$

2.4 Threshold Polarization

In general, the cross sections $Q_{|M_L|}$ are difficult to calculate, but one can assert that as the energy of the incident electrons is reduced to approach the threshold value, Q_1/Q_0 approaches zero. If this is so, the polarization near threshold is completely determined and is 15/41 = 36.6% in the case of ^3P-^3S multiplets. The justification for this assertion is as follows. The initial state of the electron-atom system has its z component of orbital angular momentum equal to zero, and therefore this must be true of the final state also, under our previous assumptions.

i.e. $M_L + m_\ell = 0$ (3)

If the energy of the scattered electron is sufficiently small, the scattered electron must be in an S state, because otherwise its impact parameter would be impossibly large. If this is so, then we have $m_\ell = 0$, and therefore $M_L = 0$ also. Therefore Q_1/Q_0 approaches zero.

The predicted threshold polarizations for several types of transitions in helium are shown in Table I.

In view of the fact that measurements have in several cases failed to show a polarization near threshold as high as predicted, it is worthwhile considering where the assumptions leading to the predictions may be vulnerable. Two possibilities come to mind.

TABLE I

THEORETICAL THRESHOLD POLARIZATIONS

Spectral Line	Threshold Polarization
$^1S - {}^1P$	0%
$^1P - {}^1S$	100%
$^1D - {}^1P$	60%
$^1F - {}^1D$	50%
Multiplet	
$^3S - {}^3P$	0%
$^3P - {}^3S$	36.6%
$^3D - {}^3P$	31.7%

(i) The range in energies over which electrons are scattered in pure S waves may be smaller than the energy width of the electron beam. The radius of an excited Helium atom is 5 or 10 Å, (depending on the state). The impact parameter of a 0.1 e.v. electron is 6 Å, so the threshold prediction is not dependable for energies much larger than this. An electron beam from a thermionic cathode has, at best, an energy resolution of about 0.2 volts. It is in fact with this consideration in mind that the 2^3P state was chosen for study. A helium atom in an n=2 state is smaller than one in an n=3 or higher state.

(ii) The factor by which the spin-orbit time is larger than the collision time is not overwhelmingly large, and requires closer examination. The numbers given in Table II are very rough, but they provide some idea of the size of the quantities involved. The collision time is calculated for the largest electron energy for which the scattered electron should be predominantly in an S state, and is compared with the spin-orbit interaction time.

TABLE II

COMPARISON OF COLLISION AND SPIN-ORBIT INTERACTION TIMES

	Symbol	2^3P	3^3P
Atomic Radius	R	5Å	12Å
Energy for Impact Parameter - R and - 1.	E	0.15 e.v.	0.03 e.v.
Velocity Corresponding to E	v	2.3×10^{7} cm./sec.	1.0×10^{7} cm./sec.
Frequency of 1 - 0 f.s. Transition	f	2.8×10^{10} H_z	8.1×10^{9} H_z
Spin-Orbit Interaction Time $1/2\pi f$	τ_{ls}	6×10^{-12} sec.	2×10^{-11} sec.
Collision Time R/v	τ_c	2.2×10^{-15} sec.	1.2×10^{-14} sec.
Ratio	τ_{ls}/τ_c	3×10^{3}	2×10^{3}

The value R is estimated from a plot of electron density in the hydrogen atom. E and v are simply taken from the Bohr formula.

The ratio of spin-orbit time to collision time seems to be large enough to allow the figures in the table to be adjusted by as much as a factor of 10 perhaps, and still leave the assumption intact that spin coordinates are not involved in the collision process. Notice, however, that especially for the 3^3P level, it is possible that the threshold polarization holds up to only very small energies above threshold.

2.5 2^3P Polarization Calculations

Massey and Moiseiwitch have done a distorted wave calculation of excitation cross sections to the 2^3P level of helium. They make predictions for the polarization of light in the 2^3P_2 - 2^3S line. In order to compare these predictions with experimental polarizations, it is necessary toconvert them to polarizations of the 2^3P - 2^3S multiplet.

Fortunately, there is a one to one correspondence between P and Q_1/Q_0, and this is easily done. The conversion formula is

$$P = \frac{\frac{G(h_1' + h_0')}{h_0 h_1' - h_1 h_0'} P'}{\frac{G'(h_1 + h_0)}{h_0 h_1' - h_1 h_0'} + P'} \qquad (25)$$

where P is the multiplet polarization and P' is the line polarization. The values obtained are plotted along with the experimental data in Figure 28.

2.6 Depolarization due to a Magnetic Field

The polarization of light from an atom depends on the relative populations of the magnetic states of the excited level. A magnetic field directed at right angles to the quantization axis will tend to mix the magnetic states, and if this magnetic field has a component in the direction of observation, the polarization is decreased. This depolarization is known as the Hanle effect and is described by Mitchell and Zemansky.[4] If the directions of observation and of the magnetic field are the same, the reduction in polarization is given by

$$\frac{P}{P_o} = \frac{1}{1 + \left(\frac{e}{mc} H g \tau\right)^2} \tag{26}$$

where H is the magnetic field and τ is the radiative lifetime of the excited state. For the lines studied in this thesis we have

$$\frac{P}{P_o} = \frac{1}{1 + (2.9\, H)^2}$$

where H is measured in gauss.

If we want the depolarization to be less than 1%, say, we must reduce any transverse magnetic field to less than 3.5×10^{-2} gauss.

2.7 Polarization as a Function of Angle

In the theory of the polarization of light due to electron impact on atoms, we assumed that the observer looks from a direction at right angles to the electron beam. But in practice, the observer looks at a cone of light rays. In this section we find how the polarization varies with the angle of observation.

We consider the light radiation to originate from three mutually perpendicular dipole antennae. The z axis antenna radiates with intensity I'' in a direction perpendicular to its axis, and the x and y antennae each radiate with intensity $I^{\perp}$ in directions perpendicular to their axes. The radiation intensity from a radiating dipole varies as $\sin^2\theta$, where θ is measured from the dipole axis.

If we look at the light at an angle α from the perpendicular to the electron beam, the polarization we see is

$$P(\alpha) = \frac{I'' \cos^2\alpha + I^{\perp}\sin^2\alpha - I^{\perp}}{I'' \cos^2\alpha + I^{\perp}\sin^2\alpha + I^{\perp}}$$

$$= \frac{(I'' - I^{\perp})\cos^2\alpha}{I'' + I^{\perp} - (I'' - I^{\perp})\sin^2\alpha}$$

$$P(\alpha) = P(0)\ \frac{\cos^2\alpha}{1 - P(0)\sin^2\alpha} \tag{27}$$

If α is small, this becomes

$$P(\alpha) = P(0)\left[1 - (1 - P(0))\alpha^2\right]$$

The total effect on the observed polarization is found by averaging over the directions of observation.

2.8 Intensity as a Function of Angle

Not only the polarization, but also the intensity of light varies with the angle of observation. If θ is the angle from the z axis, the intensity is given by

$$I(\theta) = I'' + I^{\perp} - (I'' - I^{\perp})\ \cos^2\theta$$

$$I(\theta) = I(\pi/2)(1 - P\cos^2\theta) \tag{28}$$

(We have used the same model as in the previous section.)

The total intensity is

$$I = 2\pi\int_0^{\pi} I(\theta)\sin\theta\, d\theta = 4\pi I(\pi/2)\left[1 - P/3\right] \tag{29}$$

The importance of this relationship is that in order to measure collision cross sections by measuring light intensities in a direction perpendicular to the electron beam, one must know the polarization of the light.

2.9 Effect of Dispersion of Electron Beam on Polarization

If the axis of polarization is rotated by angle θ, the new polarization is

$$P' = \frac{I'' \cos^2\theta + I^\perp \sin^2\theta - I'' \sin^2\theta - I^\perp \cos^2\theta}{I'' + I^\perp}$$

$$= \frac{I'' - I^\perp}{I'' + I^\perp} (\cos^2\theta - \sin^2\theta)$$

$$= P(1 - 2\sin^2\theta) \qquad (30)$$

For small angles, this becomes

$$P' = P(1 - 2\theta^2)$$

The total effect on the observed polarization is obtained by averaging over the velocity directions in the electron beam.

References and Footnotes for Chapter II

1. I. C. Percival and M. J. Seaton, Phil. Trans. Ser. A 251, 113 (1958).

2. E. U. Condon and G. H. Shortley, The Theory of Atomic Spectra, (Cambridge University Press, London, 1963)

3. H.S.W. Massey and B. L. Moiseiwitch, Proc. Roy. Soc. (London) Ser. A 258, 147 (1960).

4. A.C.G. Mitchell and M. W. Zemansky, Resonance Radiation and Excited Atoms (Cambridge University Press, London, 1961).

CHAPTER III

EXPERIMENTAL DETAILS

3.1 Vacuum System

The vacuum system is shown in Figure 4. The various parts are demountable, being joined by nuts and bolts and sealed with neoprene "O" rings. It is a conventional system, for the most part, and it is possible to obtain pressures as low as 2×10^{-7} torr with it.

The main pump is an oil diffusion pump (Balzers, Diff. 170) with a speed of 90 litres/second with the baffle in place. The diffusion pump is backed by a mechanical pump (Welch 1402) with a pumping speed of 100 litres/minute. In series with the diffusion pump is a water cooled baffle which reduces oil backstreaming, and a liquid nitrogen trap. The trap was fitted with a copper collar that was kept cold by thermal conduction through a copper rod from the inner part of the trap. The purpose of this collar was to discourage oil creep along the warm outside walls of the trap. When low energy electron beams are being used it is important to keep oil out of the vacuum system, because oil can be deposited as an insulating layer which will charge up to large potentials. When the vacuum pumps were operating, the trap was always kept cold. A filling of liquid nitrogen

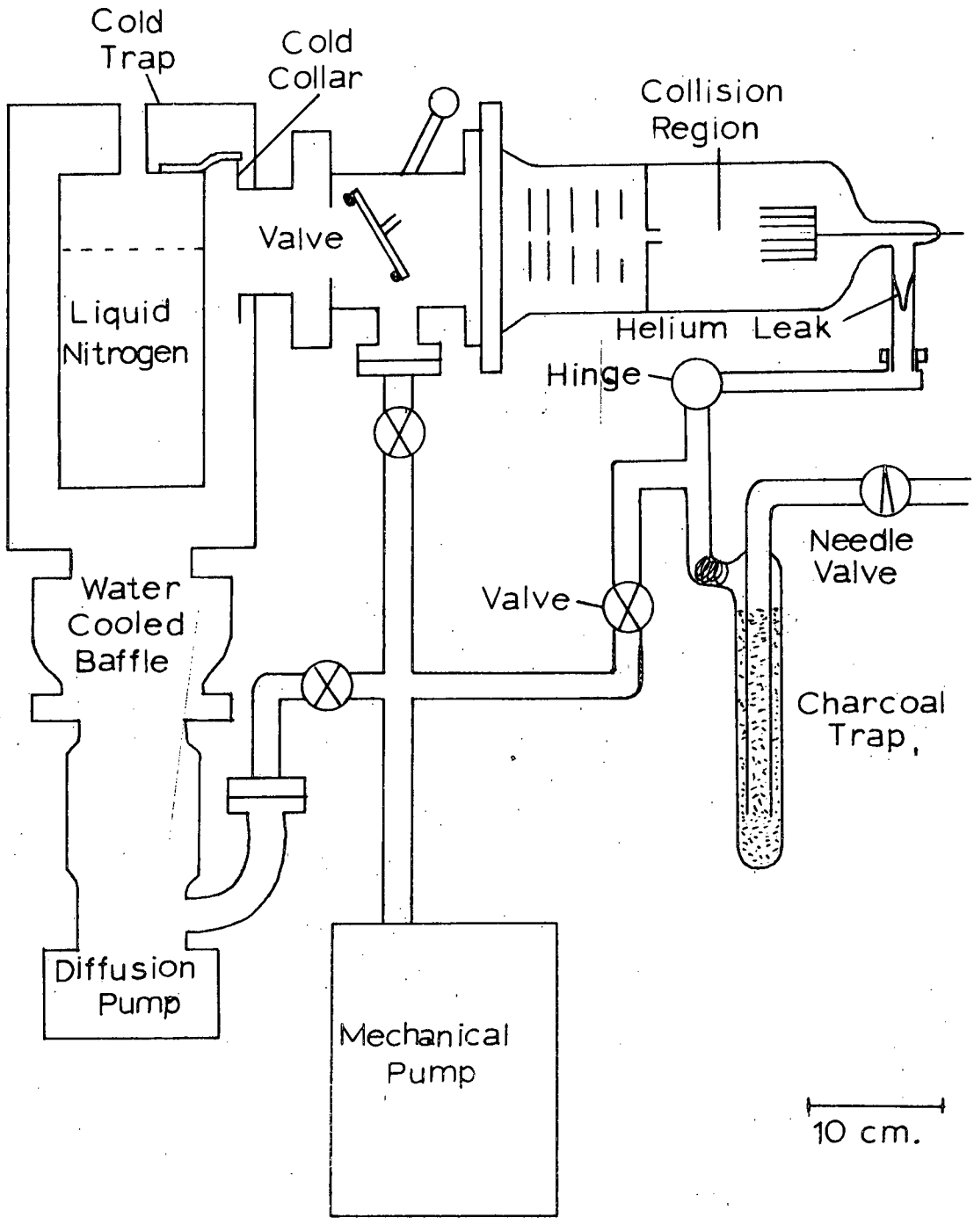

Fig. 4. Vacuum System. The components are drawn to scale, but the vacuum connections are schematic only.

lasted for about 16 hours. Normally the trap was filled twice daily.

The next component upstream from the liquid nitrogen trap is a plate valve. It was useful during the preliminary stages of the experimental work when the vacuum chamber had to be opened often. It was not used once the experiment was working. However, the ports in the valve housing were used. One port was used for rough pumping, and another was used for electrical wires. The electrical connections into the vacuum were made through glass insulated feed-through components that were soldered to a brass plate.

The vacuum chamber was made from a piece of industrial pyrex pipe, with 4 inches nominal inside diameter. It was bolted to a brass flange and sealed with an "O" ring. The chamber could be supported from below and removed whenever it was necessary to change anything inside. The electron gun mount slides into the vacuum chamber and the end wall of the mount divides the chamber into two sections. One section contains the electron gun, and the other is the collision region. (See Figure 5)

The hole connecting the two sections has a conductance of 0.6 litres/sec. for helium. The pumping speed for helium at the position of the vacuum chamber is estimated to have been 60 litres/sec. Hence when helium was admitted to the collision region, the pressure ratio between

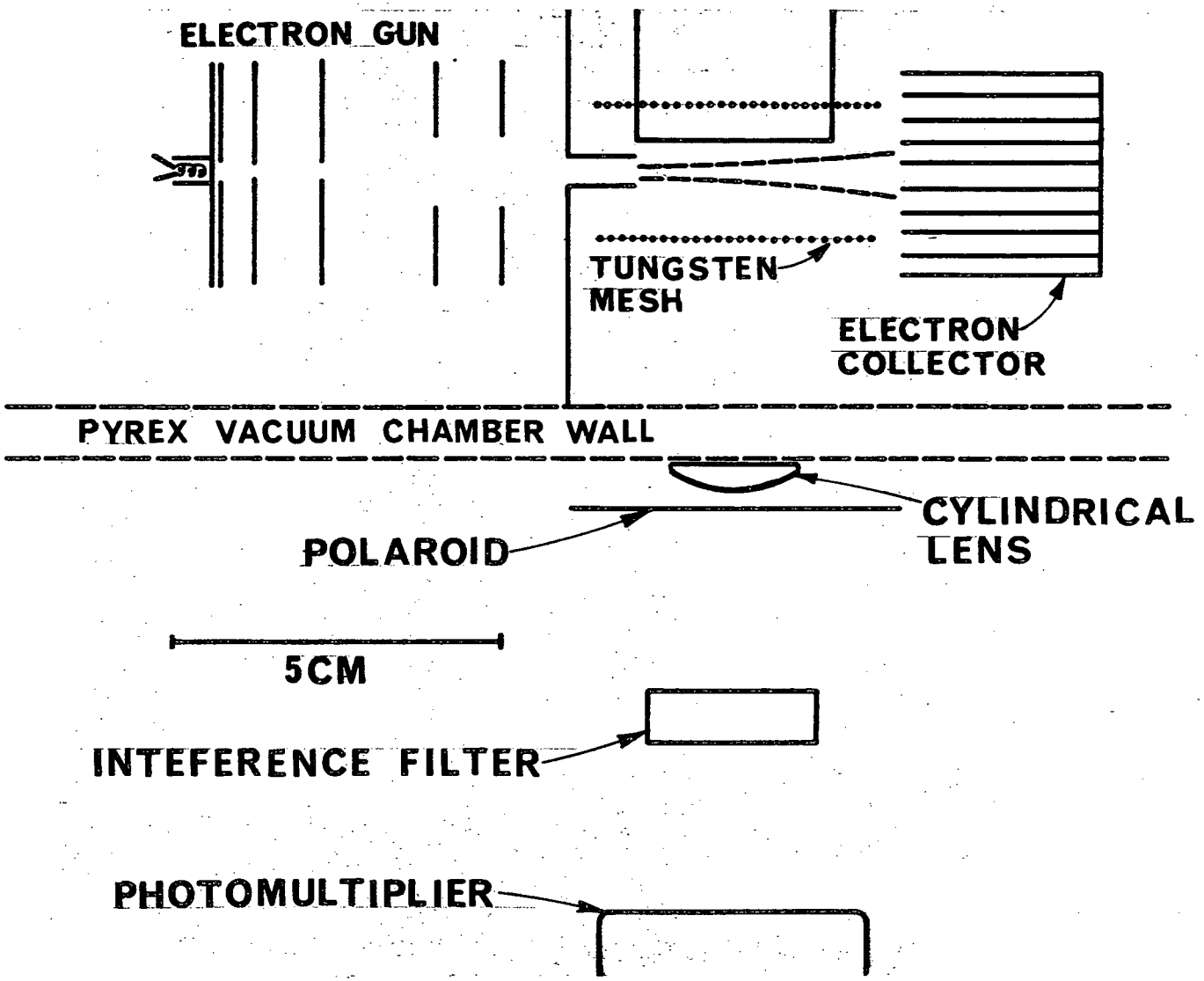

Fig. 5. Arrangement of Apparatus

the collision region and the section containing the electron gun was approximately 100/1. Because the pumping speed out of the collision region was small, that part of the vacuum chamber had to be baked in order to achieve low pressures. Baking at 120° C for a day or two was sufficient to allow the pressure to go down to 5×10^{-7} torr, as measured by an ionization gauge. If the baking was continued longer, or if the pumps were left running for a number of weeks, the pressure would go down to 2×10^{-7} torr.

Pressures were measured with a Bayard-Alpert type ionization gauge (Veeco RG-75P). This gauge was calibrated against a McLeod gauge when the polarization experiments were finished. The calibration curve is shown in Figure 6.

3.2 Helium Source

Tank helium was used. It is said by the supplier (Liquid Air Co.) to be 99.5% pure. This was evidently not good enough for this experiment, since near the excitation threshold, the impurity light was at least as intense as the helium light. The helium was therefore purified by passing it through a liquid nitrogen cooled charcoal trap. This proved to be an effective enough procedure that the impurity level was very small, and was probably determined by the cleanliness of the vacuum system.

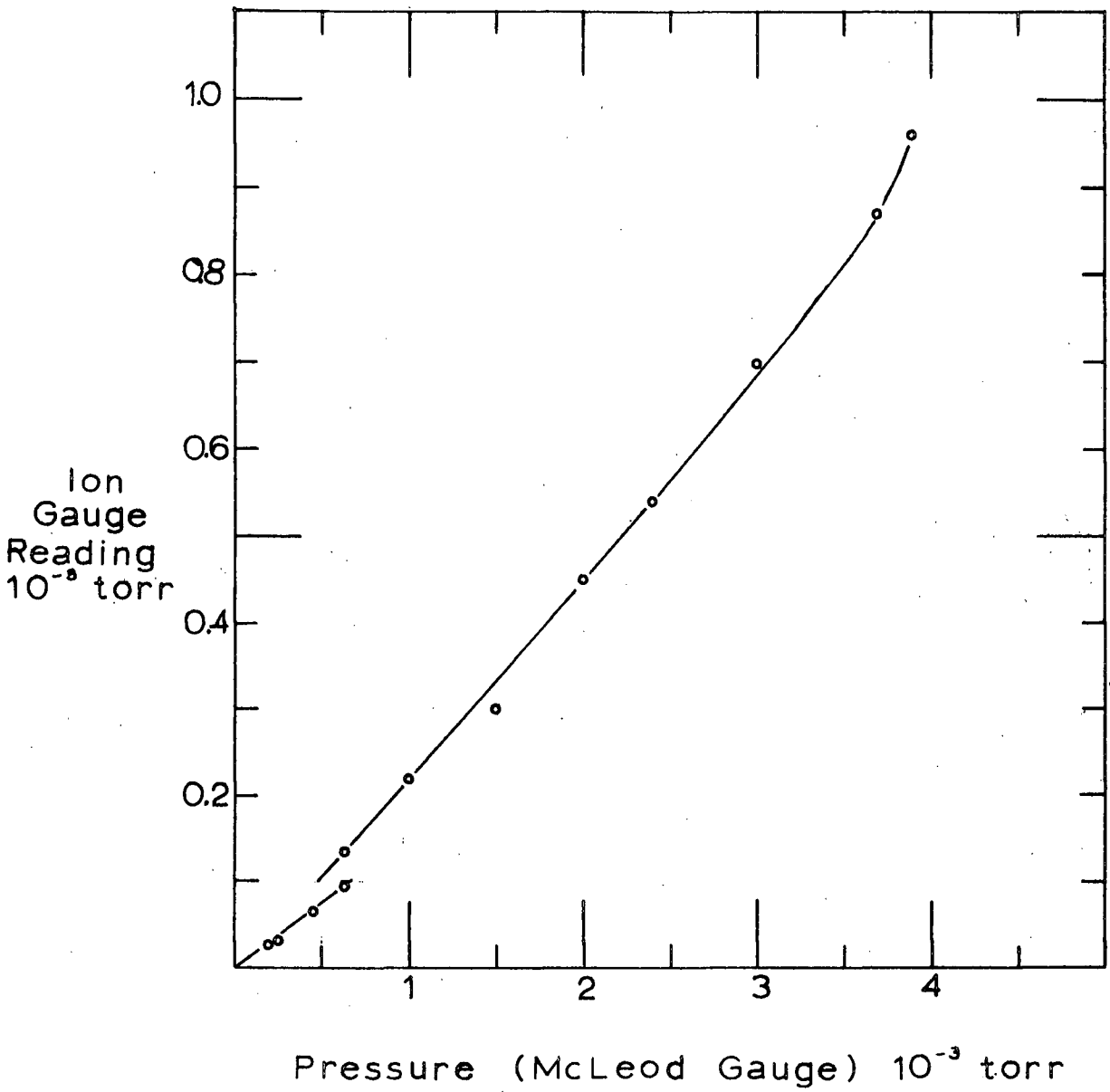

Fig. 6. Ion Gauge Calibration for Helium. The ion gauge readings correspond to a factory calibration for dry nitrogen.

The helium from the tank was admitted by means of a needle valve through the charcoal trap into a reservoir region with a volume of roughly one litre where it was left at a constant pressure of up to 0.5 atmospheres during a run of several hours. The helium passed from the reservoir into the collision region through a very fine glass capilliary leak, made by drawing out a piece of capilliary tubing in a flame. A pressure of 0.5 atmospheres in the reservoir gave rise to a pressure of about 4 millitorr in the collision region.

3.3 Electron Gun - Design and Operation

The electron gun is shown in Figure 7. It was made according to a design by Simpson and Kuyatt.[1] In this experiment the requirement is for an electron gun that will produce a stable, well defined electron beam at low energy, and with as high a current as possible. At low energies, the current density is limited by the dispersive effect of space charge. An example of the magnitude of this effect which is relevant to the electron gun that was used is the following. A 25 volt, 10μA, electron beam with a diameter of 2 mm. will, in a length of 4 cm. be dispersed to an extent that the electrons at the edge of the beam will be moving at an angle of 0.05 radians from the beam axis. (The derivation of this quantity is given in Appendix IIIA.)

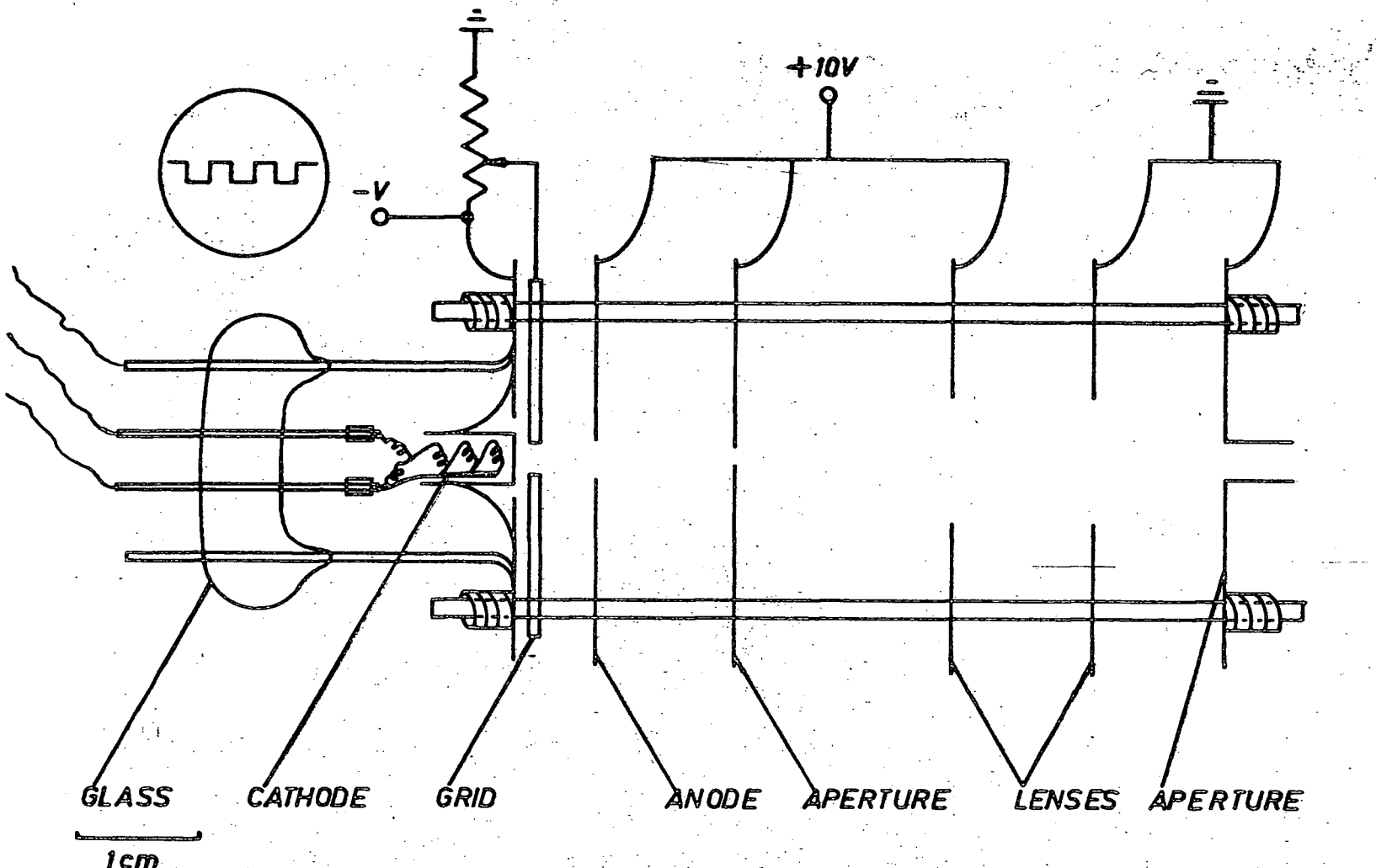

Fig. 7. Electron Gun.

It will be seen later that the observed behaviour of the electron beam at its best is consistent with this picture. Because of the space charge effect, there is a definite upper limit to the amount of current that can be forced through a given space at a given energy by electrostatic focusing.[2] The electron beam can be confined magnetically, but the author considers a magnetic field objectionable, because in a polarization experiment it is the direction of the electron's velocity that is important rather than the electron's position. A magnetic field confines the position of the electrons, but allows the electrons to move in a spiral motion with a velocity component perpendicular to the electron beam.

The design of the electron gun used here is intended to put the maximum possible current into a beam of given dimensions. It does this by first accelerating the electrons to 10 times their final energy in order to draw sufficient current from the outside, and then decelerating them and projecting them into the electron beam at the proper angles.

Voltages were applied to the plates of the electron gun as indicated in the figure. The grid potentiometer was left at a constant setting such that the potential difference between the cathode and grid was 8% of the cathode potential. The anode potential was adjusted as necessary to be 10 times the magnitude of the cathode potential. (It really should have been 9 times, but the change made very little difference

in the beam shape.) To the cathode was applied a square wave potential at a frequency of 500 H_z. The light from the electron beam was chopped in this way, as will be explained later. The potential applied to the cathode determines the electron energy since the collision chamber is at ground potential.

At 25 volts, the electron gun delivered from 5 to 10μA, depending on the condition of the cathode. The electron beam, which in the presence of helium could be seen with dark adapted eyes, was 2 mm. in diameter where it emerged from the gun, and spread to a diameter of 4 mm. at the electron collector which was 4 cm. away. After the gun had been in service for several weeks, the beam would spread to 1 cm. at the collector. Removing the gun and cleaning it with trichloroethylene vapour restored the original beam shape.

3.4 Electron Gun - Construction

The electron gun was made from a kit supplied by Nuclide General Corporation. It consists of stainless steel plates and ceramic spacers connected by ceramic rods. Before this kit was obtained, the author spent a large amount of time in fruitless attempts to make an electron gun. These attempts will not be described here, but a few comments may be in order.

The main point is that the number of materials that can be used at elevated temperatures in a vacuum is severely

restricted. This is particularly true of insulating materials. Ceramics and glass are about the only materials that can be used. As for metals, brass cannot be used, because of the high vapour pressure of zinc. Ordinary electrical soft solder should not be used, even below its melting point, because when it becomes warm, it sprays the vacuum chamber with metallic vapour. A ceramic material that promised to be very useful is Sauereisen Insa-Lute cement. When it is dry, it forms a hard, strong, ceramic-like body. Unfortunately, after being heated to only 120° C in a vacuum for a few days it dries out, and crumbles to powder under the slightest stress.

The chief difficulty in making electron guns, then, is the lack of a suitable insulating material that can be worked easily and precisely. This is important, because the metal parts must be aligned precisely by insulating pieces that are small and difficult to make. A suitable material that has recently become available is Boron Nitride, available from The Carborundum Co., Latrobe, Pa., U.S.A.

There appear to be three possible approaches to making electron guns for experimental work. One is to make precise insulating parts. This is what has been done at the factory in the electron gun kit. As an alternative, a suggestion by Krotkov[3] was to use synthetic sapphire balls as precision insulating spacers. A second approach

is to align the metal parts precisely on some sort of jig, and fix them in place with a plastic insulating material. This is what is done in the commercial manufacture of electron guns, in which the plastic material is glass. But this requires special equipment. A third approach is to use ready-made electron guns, from television tubes for instance. This is a good approach, of course, only if one can find a gun suitable for the experiment. Heddle and Keesing[4] used a low energy electron gun from a magnetron tube, which, however required a magnetic field to operate.

The kit solves the problem of making the electron gun, but one still has to decide what kind of cathode to use and how to attach it. To start with, the electron gun used in this experiment requires a planar cathode, and for the best energy resolution, and least thermal light, the cathode should operate at a low temperature. These criteria suggest oxide cathodes. These were tried. The disadvantage is that they are short lived in practice. They poison easily, and should be kept under continuous high vacuum. They can be taken out of the vacuum, put back, and reactivated if care is taken to keep them dry, but their emission is substantially reduced, and the procedure can be repeated at most two or three times. They also tend to make the gun a bit dirty, since the binder evaporates during activation and settles on other parts of the gun.

Dispenser cathodes were finally used. They run at a somewhat higher temperature, (1100° C as opposed to 800° C.) but they recover after poisoning, and they survive being taken to atmospheric pressure quite well. They can even be left under rough vacuum for a while without requiring reactivation. Only three dispenser cathodes were used in all.

The cathodes were mounted to a stainless steel plate by means of three tungsten wires 0.01" in diameter and 1 cm. long. The wires were spot welded with tantalum foil being used as flux. (The manufacturers recommend that only refractory metals be used at the cathode temperature to avoid poisoning the cathode.) Shorter, thicker wires were tried, but it was found that the greater heat loss necessitated heater temperatures high enough to burn out heater filaments after a few hours of operation. With the arrangement just described, however, heaters outlasted the cathodes. The heater was spot welded (with tantalum foil) to tungsten wires which were supported by a glass structure. (See Figure 7.)

The electrical leads were bare nickel wires spot welded to the stainless steel plates of the electron gun. These wires were spot welded at the other end to plug connectors made from one inch finishing nails cemented into pieces of ceramic tubing. On the other side of the

connectors, within the valve housing which was always cool, enamelled copper wire was used.

The cathodes were activated at 1150° C brightness temperature and operated at approximately 1000° C brightness temperature. In order to find the relationship between temperature and heater current, the cathode was heated in a vacuum, without the remainder of the electron gun, and its temperature was measured with an optical pyrometer.

3.5 Electron Gun Mount

This is shown in Figure 8. The electron gun rests on ceramic rods. The rest of the mount is made of copper. The end of the electron gun is attached with screws to the wall separating the collision region from the rest of the vacuum chamber. The whole mount was made to slide in and out of the vacuum chamber, and to make a fairly close fit with it. The idea was to make the hole that the electrons passed through the only important passageway for helium between the two regions of the vacuum chamber. The fit between the electron gun and the vacuum chamber was close enough that baking at a temperature a great deal higher than 120° C would have been risky because of the expansion of the copper.

The whole assembly of electron gun and mount, except for the cathode, was cleaned with trichloroethylene vapour,

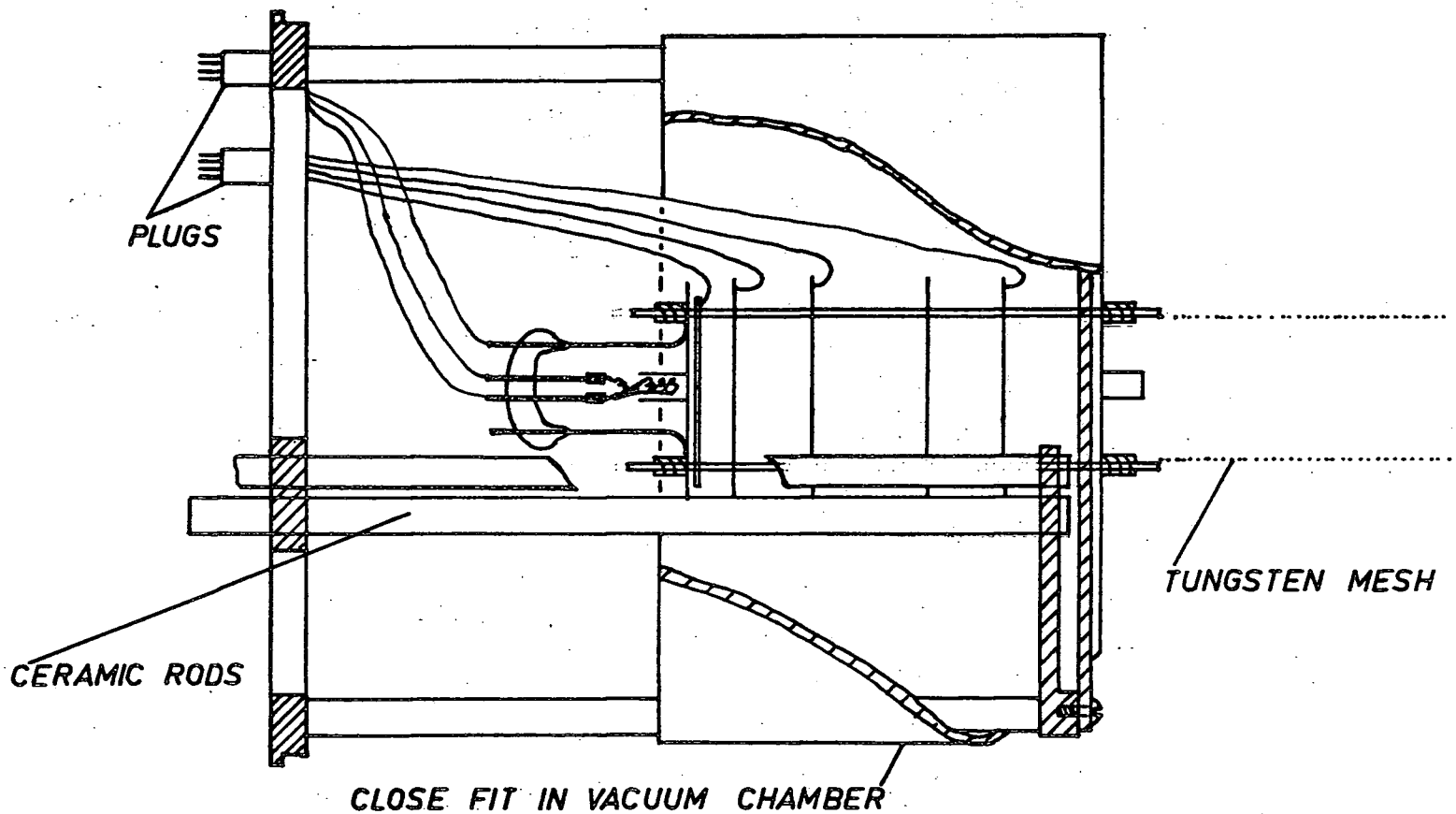

Fig. 8. Electron Gun Mount, Cutaway View.

as shown in Figure 9, just before putting it under vacuum.

3.6 Collision Chamber

Everything in the collision chamber except optical parts was coated with colloidal graphite to reduce surface charging[5] and reflections of light and electrons[6]. A grid of fine tungsten mesh 2 cm. in diameter concentric with the electron beam was used to shield the electron beam from surface charges on the viewing window.

That such surface charging was very important was shown by the following observation when the shield was not present. If one looked at the electron beam (with helium in the collision region), what was seen depended on the energy of the electrons. Up to 24 volts, nothing was seen. Then as the energy was increased, the beam would become visible at both ends, and lengthen from each end towards the middle and unite when the electron energy was approximately 30 volts. (See Figure 10.)

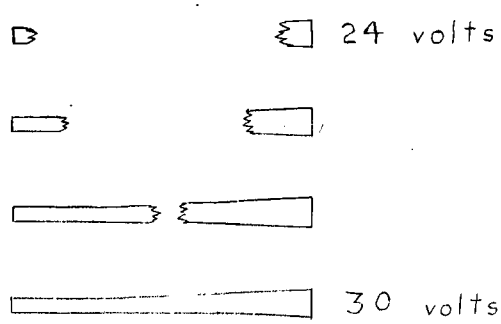

Fig. 10. Evidence of Potential Minimum.

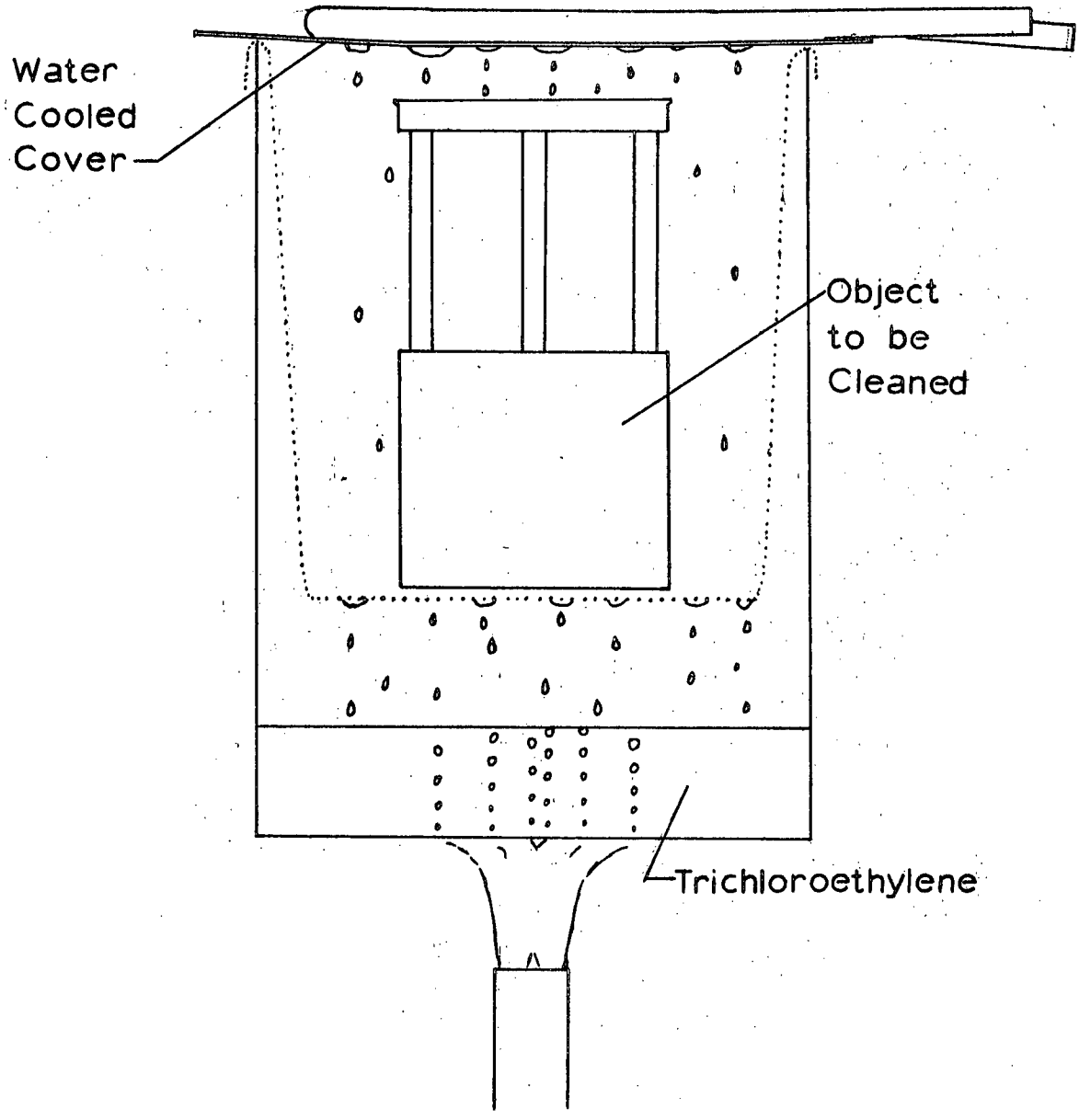

Fig. 9. "Vapour Degreasing" Method of Cleaning Vacuum Parts.

This effect is interpreted as being due to a potential gradient along the beam. The potential was 6 volts lower at the centre of the collision region than at the ends. In order to remedy this, an electrostatic shield made of wires spaced at 3 mm. intervals was placed around the beam. However it was not entirely effective. The tungsten mesh finally used has a wire spacing of 0.8 mm. and it eliminated the effect. The electrostatic potential calculations necessary to determine how fine a mesh is needed are given in Appendix IIIB.

The electron collector is a copper cup filled with fins in order to reduce electron reflections.

The vacuum chamber, except for the viewing window, was surrounded by two layers of magnetic shielding (Conetic AA, Perfection Mica Co.). The transverse magnetic field at the position of the electron beam was measured to be 0.01 gauss. The longitudinal field was of the same order of magnitude.

3.7 Optics

Because the light intensity in this experiment is small, it is important to collect as much of the light as possible, within certain limitations. One limitation is the polarization of light changes with the angle of observation (equation 27). Therefore we cannot collect

light over a large angle α. However we may collect light from as large an angle ϕ as we like. Another limitation is imposed by the size of the light detector, which is effectively about 1 cm. in diameter in this experiment. The optical system used is shown in Figure 11. The light from the excited helium is focused on the photocathode, in the plane of the electron beam by a cylindrical lens, and in the perpendicular plane by an elliptical aluminum mirror. The focal ratio of the mirror is approximately f/0.5 and that of the lens f/5. Thus light was collected from a solid angle of approximately 4% of 4π, and from an area of approximately 1 cm. (along the beam) by 2 mm. The image size of this part of the electron beam is 1 cm. x 1 cm. Thus in one plane, light is collected from a large angle and small object, and in the other plane light is collected from a small object and a large angle.

The mirror was cut from a solid piece of aluminum with a milling machine with its head tilted at the proper angle to form the desired ellipse. It was polished with "Brasso" and "Silvo". It was found that solid aluminum is not an ideal material for making mirrors because it is somewhat porous.

It should be noted that the intensity of light received from an optical system like the one just described is quite sensitive to changes in the size and shape of the

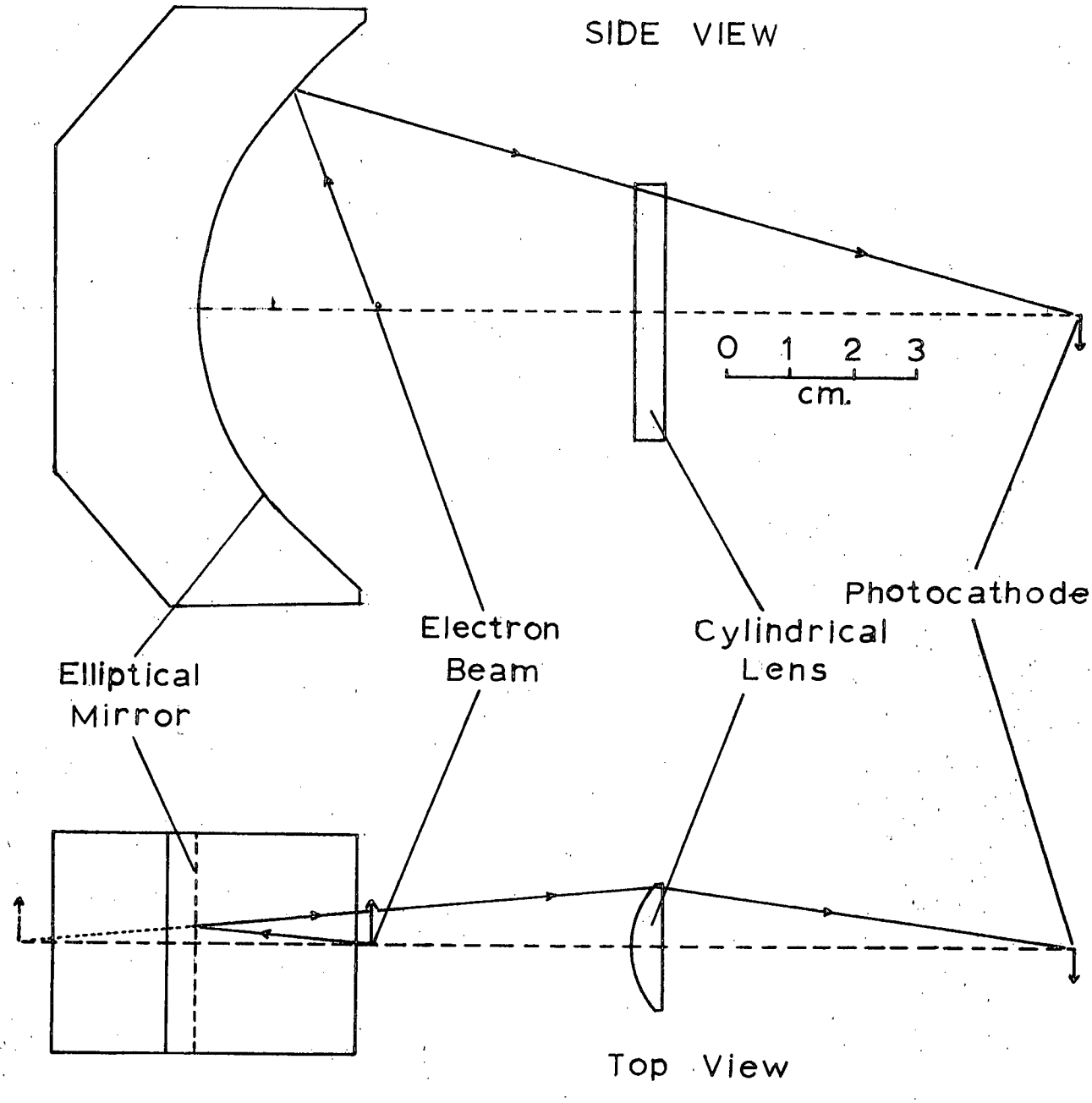

Fig. 11. Focusing Properties of Optical System.

electron beam. Therefore excitation curves obtained with it cannot be relied upon to be accurate. However, total intensity changes should not affect the accuracy of the polarization measurements.

The spectral lines were isolated with interference filters, and analysed for polarization by a sheet of polaroid which turned 90° at automatically timed intervals. Type HNP'B polaroid was used for the 3889Å line and type HR for the 10,829Å line. Transmission curves for the interference filters are shown in Figure 12 and Figure 13.

3.8 Photomultipliers

For measurements on the 3889Å line, an E.M.I. 6256S photomultiplier was used. It had a dark current of about 130 counts/sec. at room temperature and about 5 counts/sec. at 260°K. It was usually not necessary to cool it. The 6256S was operated at 1500 volts and had a gain of 2.5×10^7.

For measurements on the 10,829Å line, a Phillips CVP 150 photomultiplier selected for relatively high infrared response was used. Its quantum efficiency at 10,829Å was approximately 6×10^{-4}. It was cooled to 135°K where it had a dark current of 10 counts/sec. The CVP 150 was operated at 1420 volts and had a gain of 6.5×10^5.

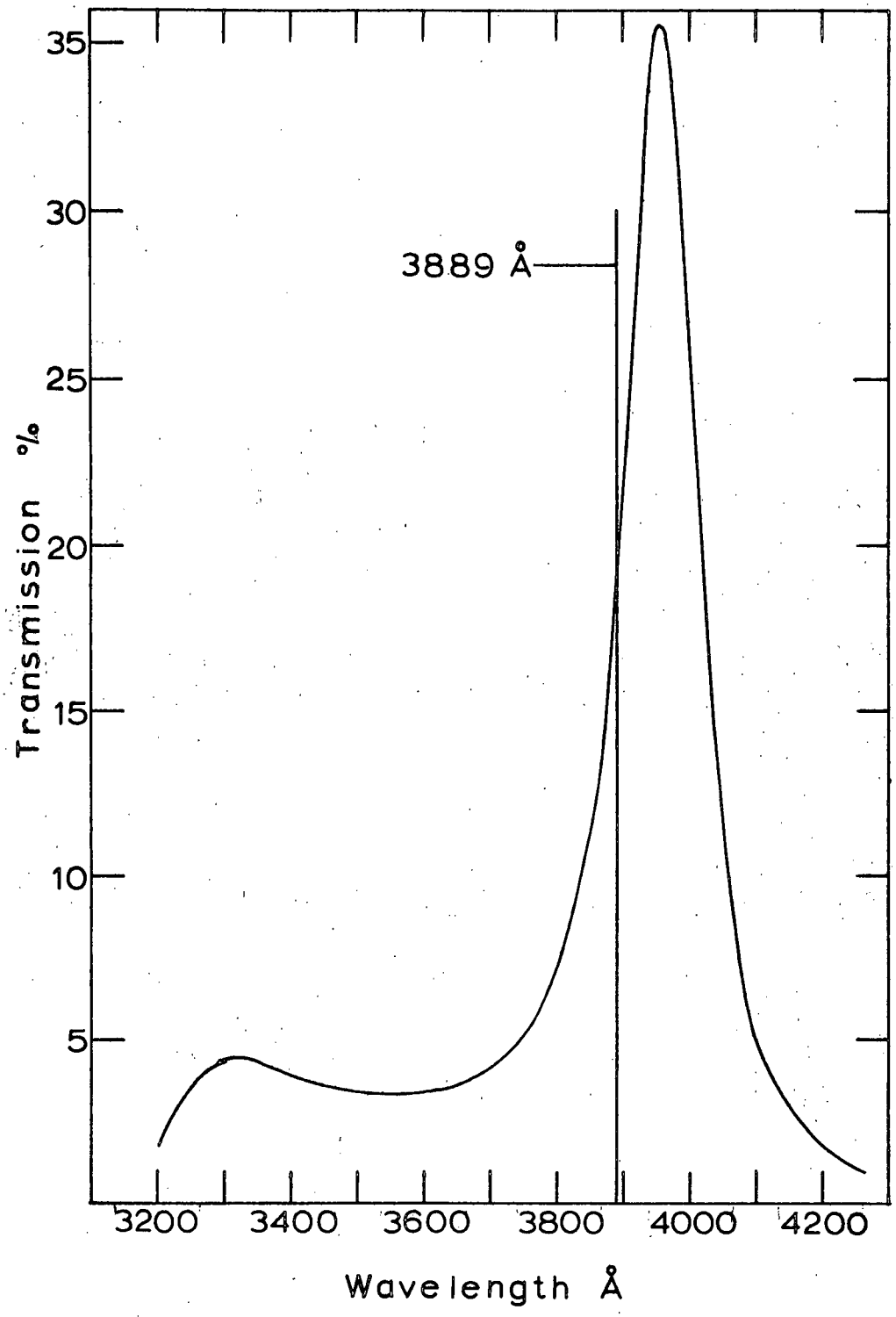

Fig. 12. Optical Transmission of Interference Filter

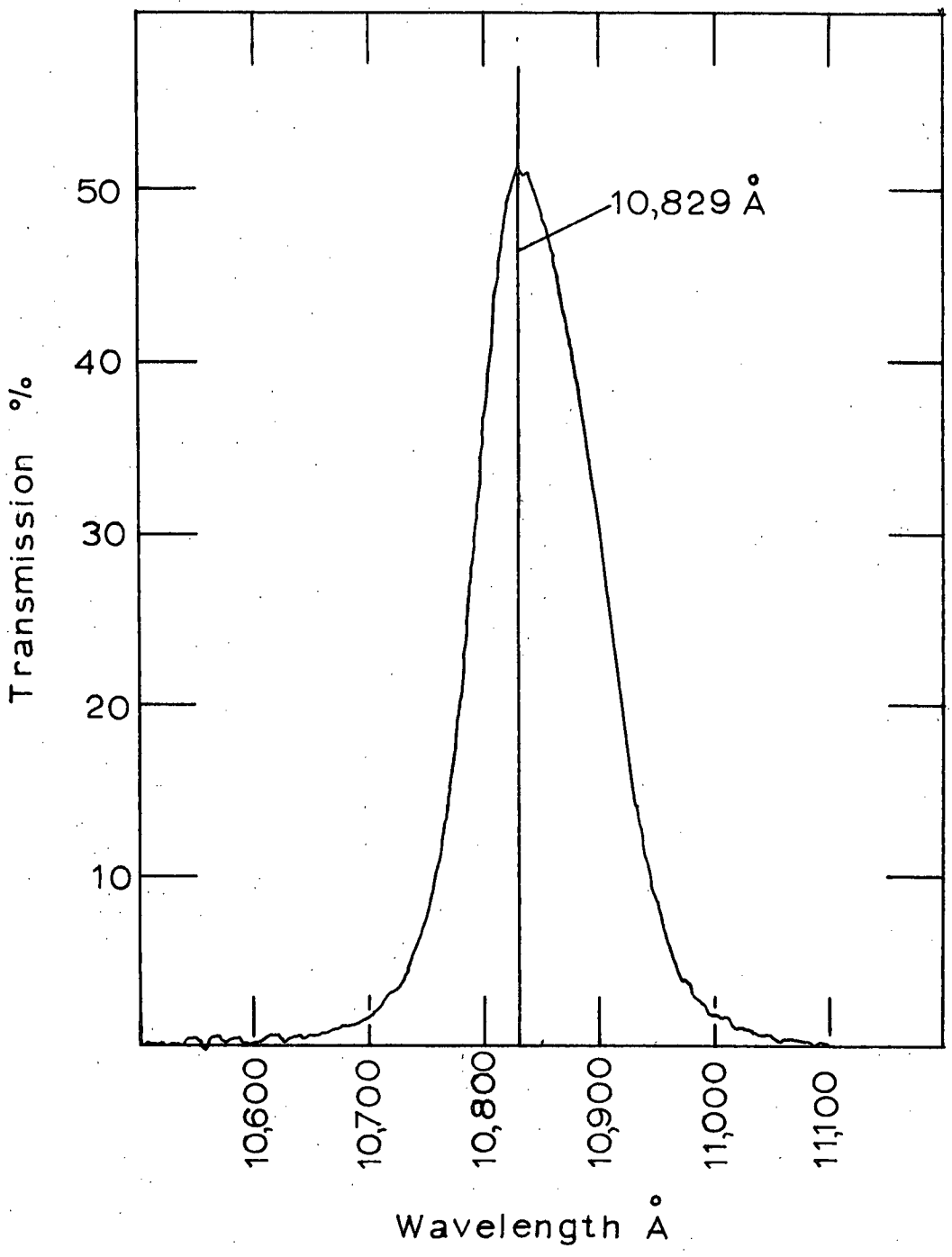

Fig. 13. Optical Transmission of Interference Filter.

3.9 Photomultiplier Cooling

The housing used to cool the CVP 150 photomultiplier is shown in Figure 14. Liquid nitrogen is boiled off, and the resulting cold, dry nitrogen is passed around the photomultiplier. A thermister attached to the photomultiplier was used to measure its temperature. The cooling device was supplied by Spex, but had to be modified somewhat. A brass sleeve was added to improve the cold nitrogen flow and to help provide electrostatic shielding. Insulation was added on the inside. Finally, in order to prevent the polaroid turner from getting cold it was necessary to warm it by passing hot water through a coil in thermal contact with it (coil not shown in diagram). The device finally operated satisfactorally down to 135°K, as measured by the thermister.

3.10 Signal Processing

A block diagram of the electronics is shown in Figure 15. The functions of the various components are described in the following sections.

Electron Gun Control. The electron gun control supplies the various potentials to the electron gun and measures the various currents. In order to separate the light due to the electron beam from stray light, the

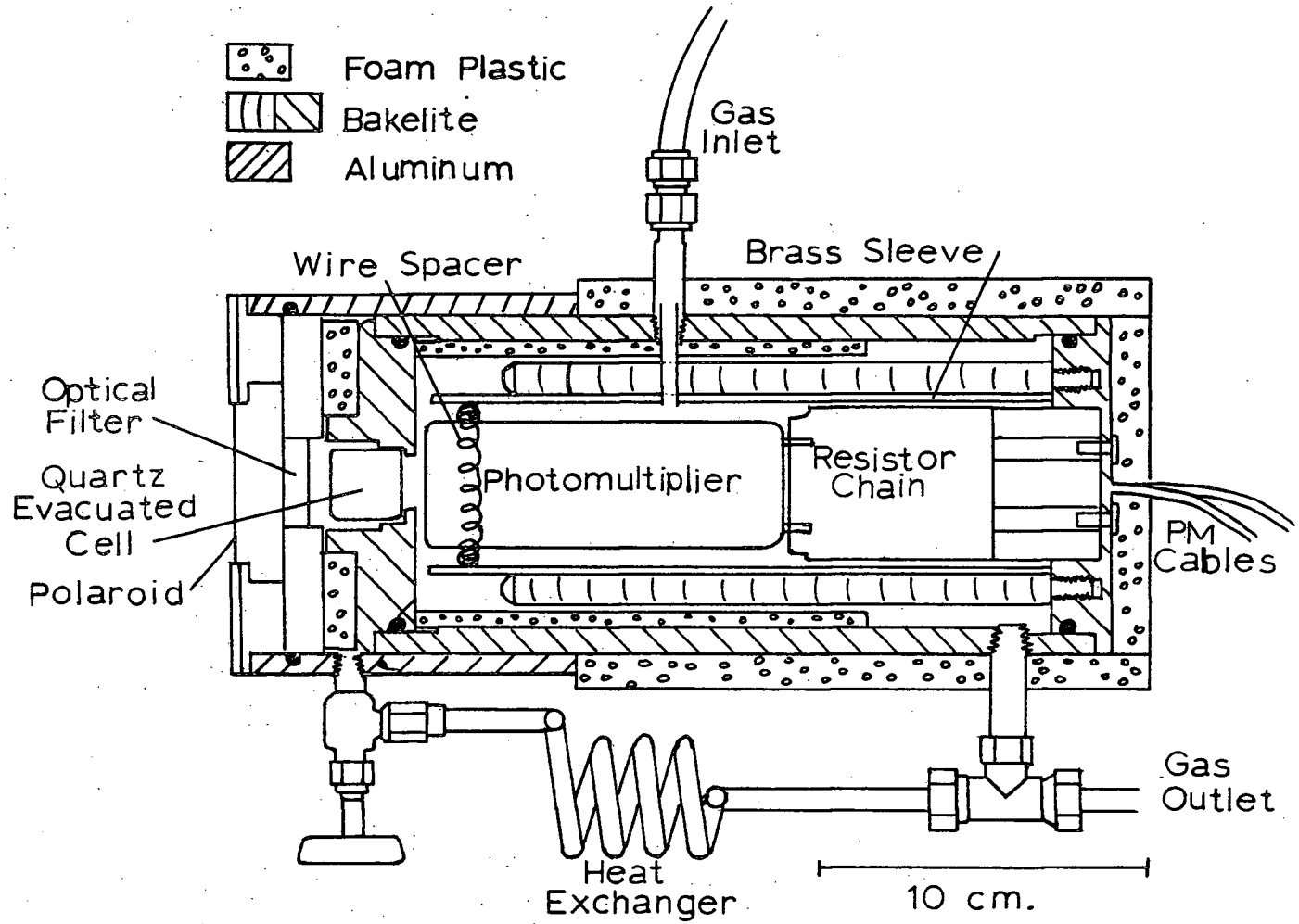

Fig. 14. Photomultiplier Cooling. The photomultiplier was wrapped in aluminum foil which was connected at cathode potential through the wire spacer.

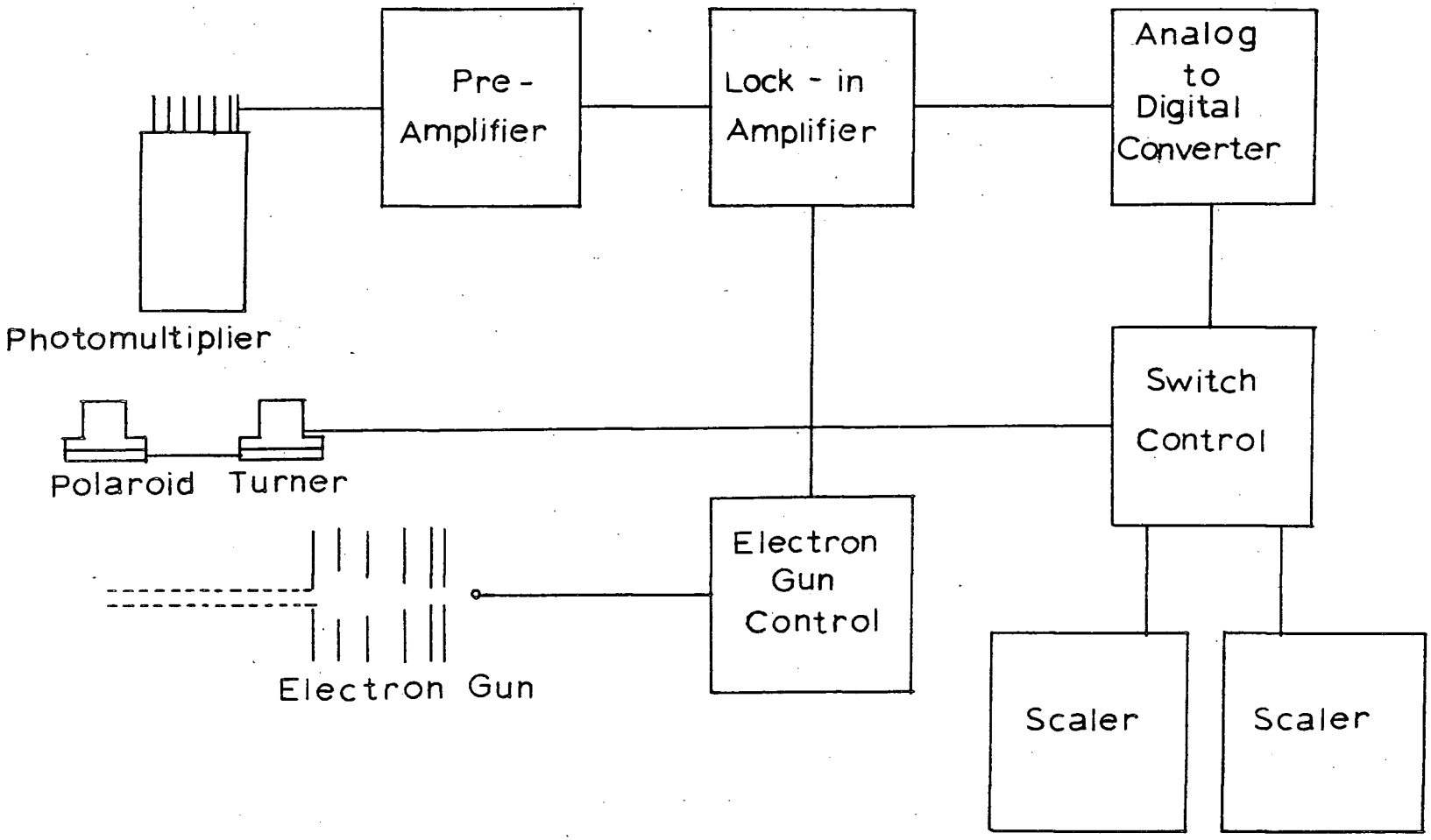

Fig. 15. Electronics: Block Diagram.

electron beam was chopped. The usual way to do this is simply to turn the beam on and off at some frequency, but in this experiment it was done in a slightly more subtle way. The beam was always on, but the energy given to the electrons alternated between the working values, and a value one or two volts below the excitation threshold. This was done to minimize the amount of background light coherent with the signal when measurements were made close to threshold. The chopping was done, then, by applying a square wave potential to the cathode. The circuit used to do this is shown in Figure 16.

Also shown is the way in which the applied potential was measured. It was compared to the potential along a precision (0.1% linearity) potentiometer, which was in turn calibrated with a mercury battery as standard.

The method of chopping made a special circuit necessary for measuring the electron beam current. It was necessary to measure the current during the "on" part of the cycle. This circuit is also shown in Figure 17.

The electron gun control also supplies the lock-in amplifier with a reference signal derived from the same oscillator that drives the cathode supply.

Preamplifier. The photomultiplier output was loaded with a 100K resistor and fed into a broadband preamplifier.

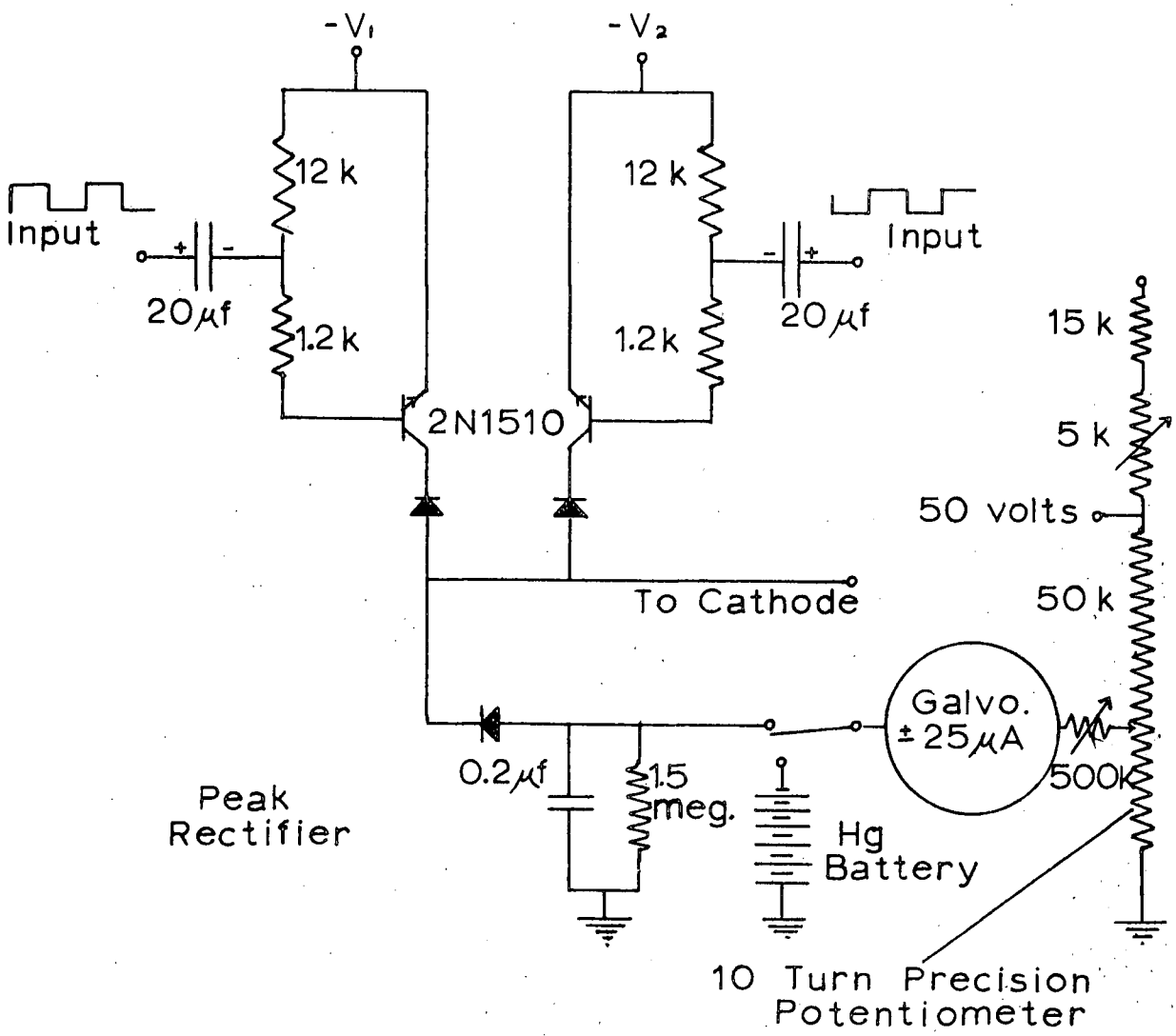

Fig. 16. Electron Gun Cathode Supply. Potentials $-V_1$ and $-V_2$ are supplied alternately to the cathode at a frequency of 500 Hz. V_1 and V_2 are independently adjustable from 0 to 50 volts. The greater of V_1 and V_2 is measured with the peak rectifier and potentiometer circuits.

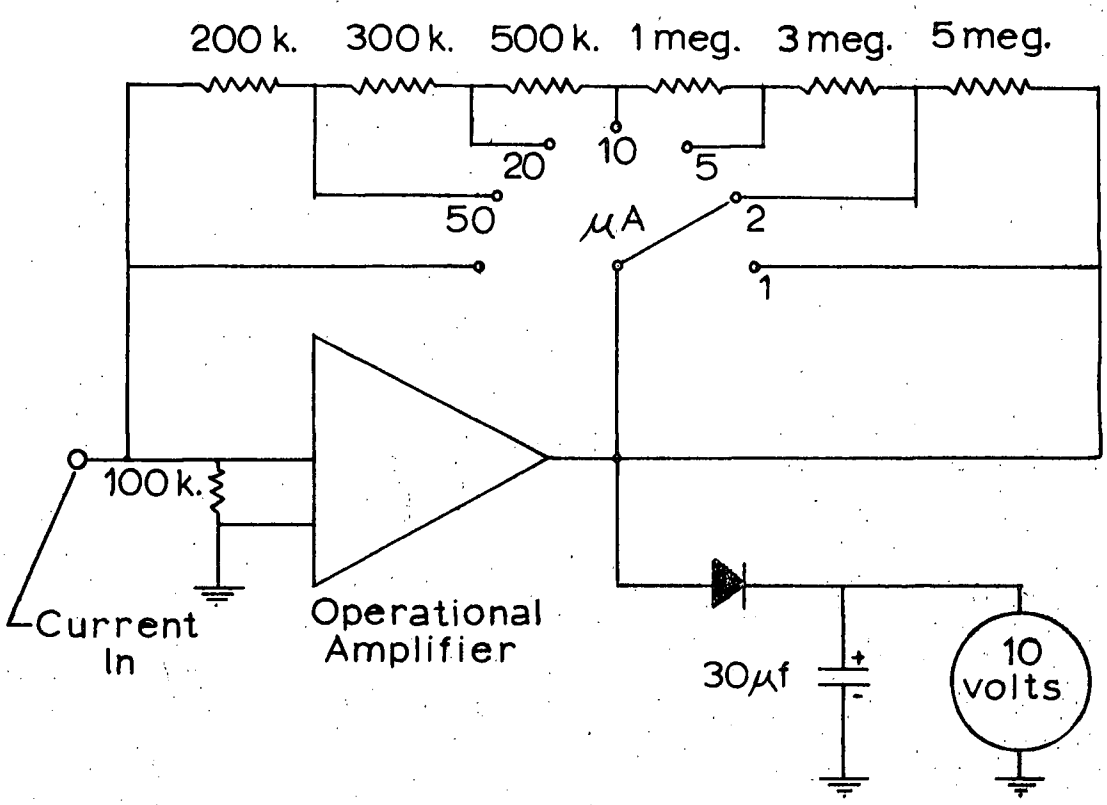

Fig. 17. Microammeter for Electron Beam. 1% accuracy resisters are used. Peak current is measured.

This arrangement had a time constant of 10^{-5} seconds. The preamplifier (Micronoise, Denro Labs) has a gain variable between 10 and 50.

Lock-in amplifier. The lock-in amplifier consists of a tuned amplifier and a phase sensitive detector. The phase sensitive detector responds only to that part of the signal that is coherent with, and in phase with the reference signal. The lock-in amplifier used in this experiment is a model JB-4, Princeton Applied Research. It has a gain of 9000 and a linearity of 1%. The output is a D.C. differential voltage which is 5 volts at full scale. In this experiment, it was used with a one second time constant.

Analog to digital converter. It was found that longer intergration times were required than were convenient to provide with RC circuits, so digital averaging was used. The analog to digital converter is a device constructed from operational amplifiers that puts out pulses at a rate precisely proportional to the potential difference applied to its input. (Linearity is 3 parts in 10^3.) Five volts gives rise to 100 pulses per second. Thus the number of pulses registered over a given time interval is a measure of the average output of the lock-in amplifier.

Switch control. The switch control determines both the position of the polaroid and the flow of signal pulses. The sequence of operations, repeated every 20 seconds, is as follows. To start with, the pulses are flowing to one scaler. Then, at a signal from the timer, the pulses are switched off, and the polaroid turns 90°. Six seconds later (the time required for transient signals to die away) the pulses are switched on again, this time going to the other scaler. In this way, arbitrarily long integration times can be achieved, and slow drifts in the total light intensity do not affect the result. In practice, integration times up to 20 minutes were used. The switch control was made up of multivibrator circuits with long time constants, and electro-mechanical relays. The timer was a free running multivibrator that completed a cycle every time the polaroid turned. Thus there was no possibility of a bias in the lengths of time given to the "parallel" signal and the "perpendicular" signal. When a constant voltage (a dry cell) was placed across the input terminals of the analog to digital converter, the scaler readings were found to be equal to within a few parts in 10^4.

3.11 Polaroid Turner

This is shown in Figure 18. It is turned by a small wheel with a friction drive. The small wheel is

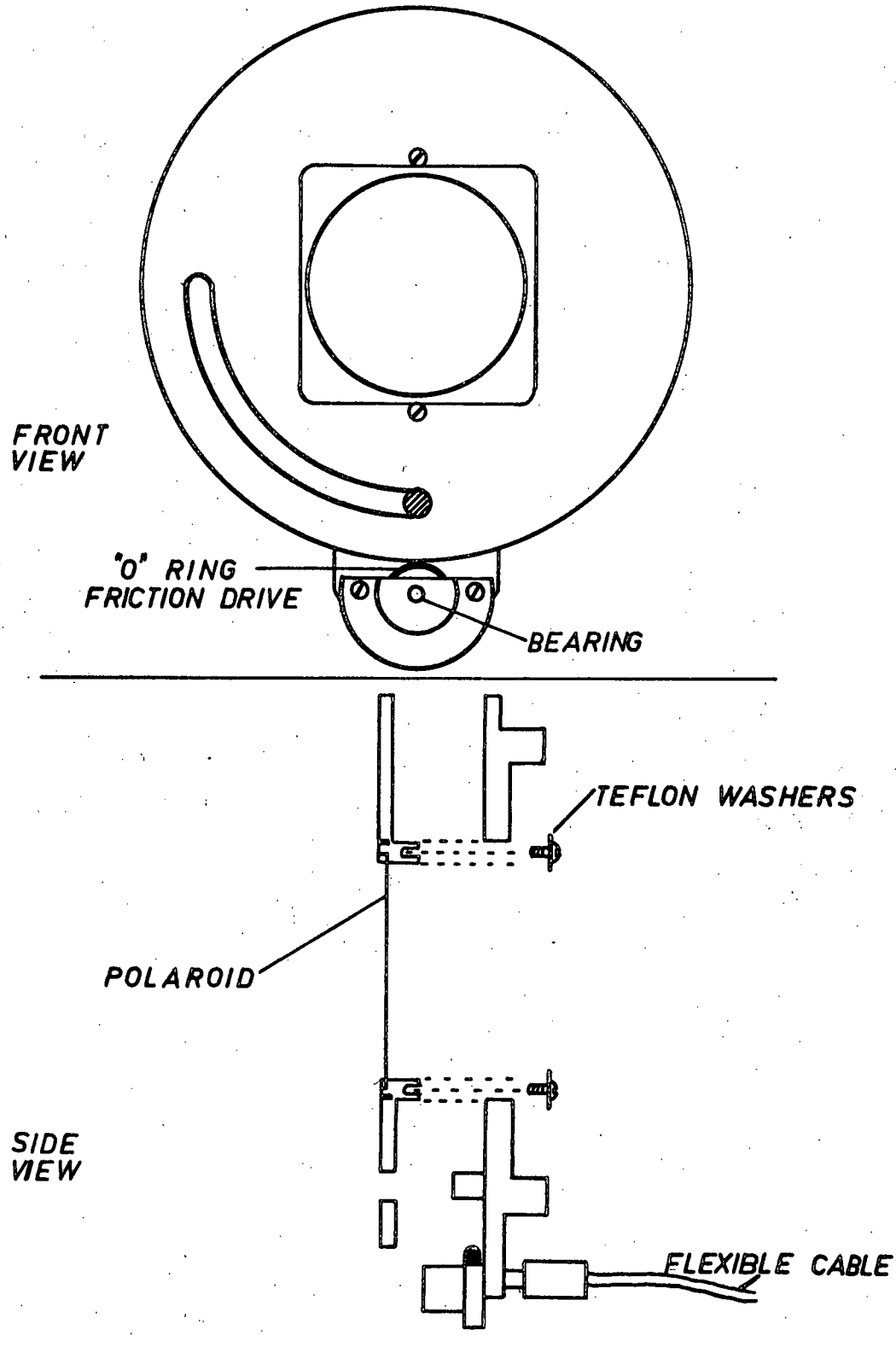

Fig. 18. Device Used to Rotate Polaroid.

driven by a flexible cable that is rotated by a reversible electric motor. The motor is turned on only during the time that the polaroid is moving.

References and Footnotes for Chapter III

1. J. A. Simpson and C. E. Kuyatt, Rev. Sci. Instr. 34, 265 (1963).

2. J. R. Pierce, Theory and Design of Electron Beams (Van Nostrand, New York, 1954).

3. R. Krotkov, Private Communication.

4. D.W.O. Heddle and R.G.W. Keesing, Proc. Roy. Soc. (London) Ser. A 258, 124 (1967).

5. E. Lindholm, Rev. Sci. Instr. 31, 210 (1960).

6. P. Marmet and L. Kerwin, Can. J. Phys. 38, 787, 1960.

CHAPTER IV

EXPERIMENTAL RESULTS

4.1 Data

The polarization of light as a function of applied potential is shown in Figures 23 to 33. Each of the eleven figures represents data taken on one day. The error bars represent r.m.s. statistical errors only. These were determined from estimates of photelectron pulse rates. No corrections have been applied to the data. The vertical dashed lines at the bottom of some of the graphs indicate "off" voltages used. (See section 3.10) The theoretical curve in Figure 28 is derived from values given by Massey and Moiseiwitch[1] as the result of a distorted wave calculation (see section 2.5). The curves drawn through the polarization data near threshold are taken from the threshold polarization model which will be discussed later, and have been fitted to the data.

The "excitation" data are simply plots of $I'' - I^{\perp}$ divided by the electron beam current. They are plotted in order to give some idea of the light intensity, and because they are of some intrinsic interest. The excitation scale is arbitrary and is not shown on the graphs. Among the

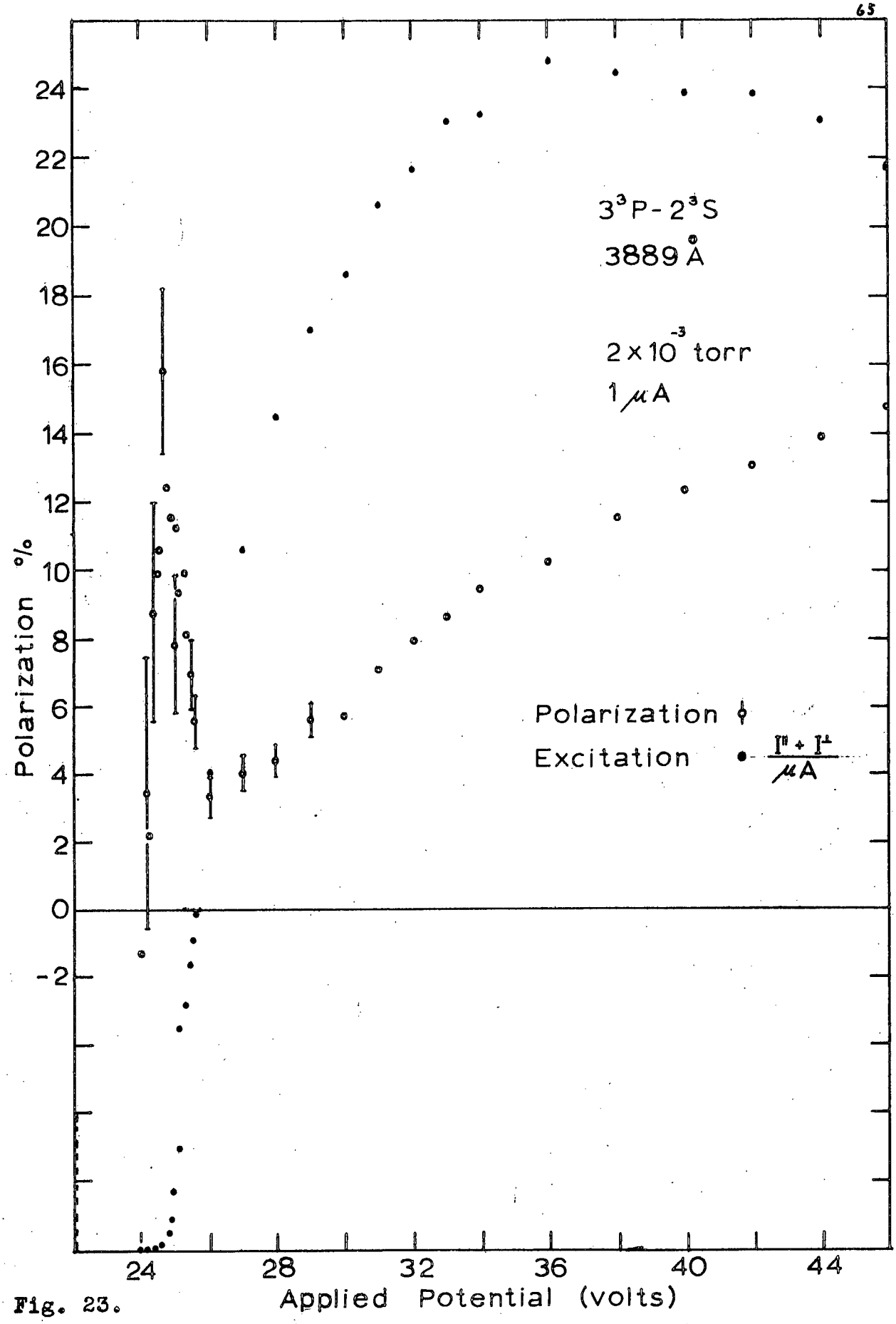
24
22
20
18
16
14
12
10
8
6
4
2
0
-2
Polarization %
24
28
32
36
40
44
Applied Potential (volts)
3^3P-2^3S
3889 Å
2×10^{-3} torr
1 μA
Polarization
Excitation
$\frac{I^{\parallel}+I^{\perp}}{\mu A}$

Fig. 23.

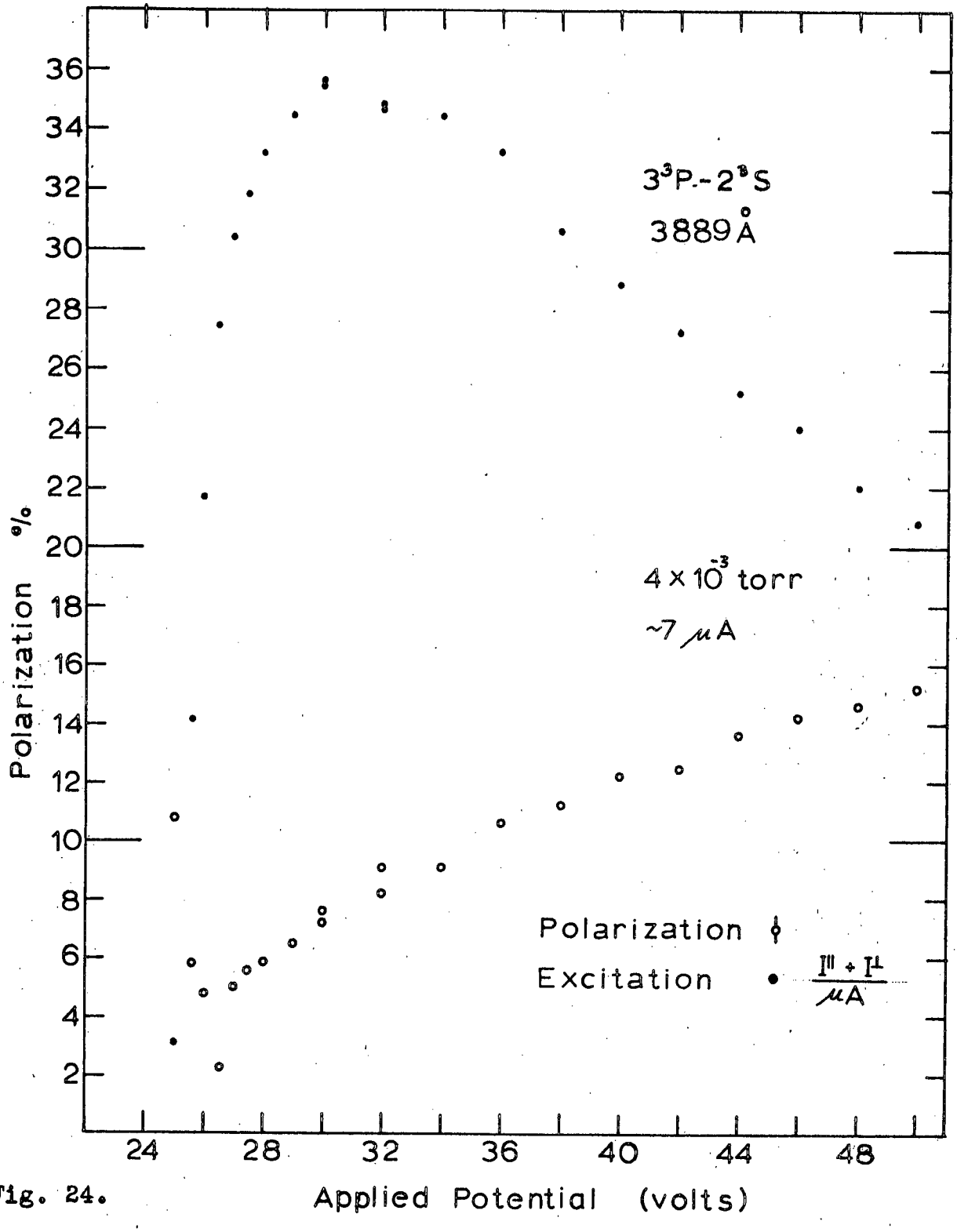
3^3P-2^3S
3889 Å
4×10^{-3} torr
~7 μA
Polarization
Excitation
$\frac{I^{\parallel} + I^{\perp}}{\mu A}$
Polarization %
Applied Potential (volts)
36
34
32
30
28
26
24
22
20
18
16
14
12
10
8
6
4
2
24
28
32
36
40
44
48

Fig. 24.

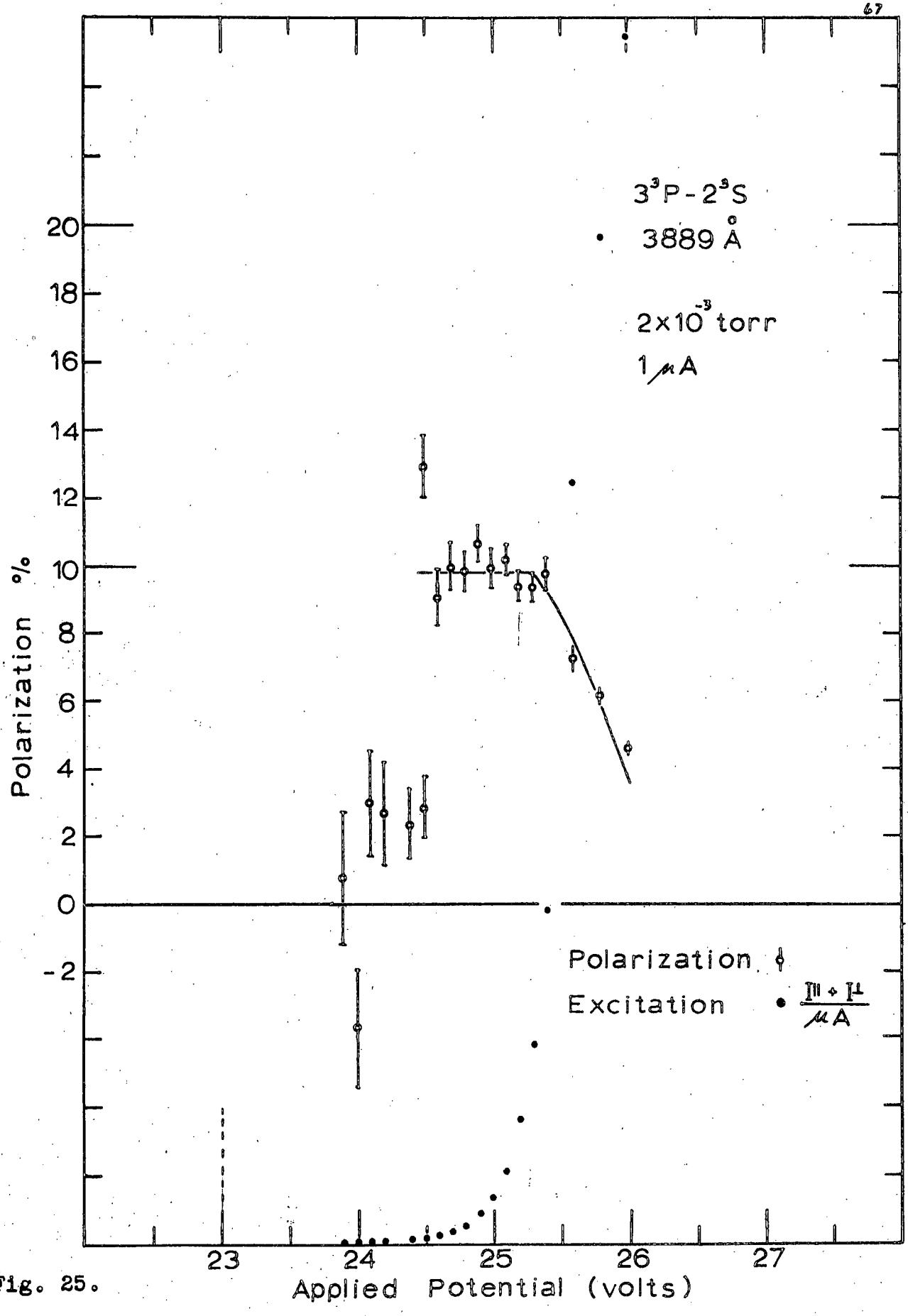
3³P - 2³S
3889 Å
2x10⁻³ torr
1 μA
Polarization %
20
18
16
14
12
10
8
6
4
2
0
-2
Polarization
Excitation
I∥ + I⊥ / μA
23
24
25
26
27
Applied Potential (volts)

Fig. 25.

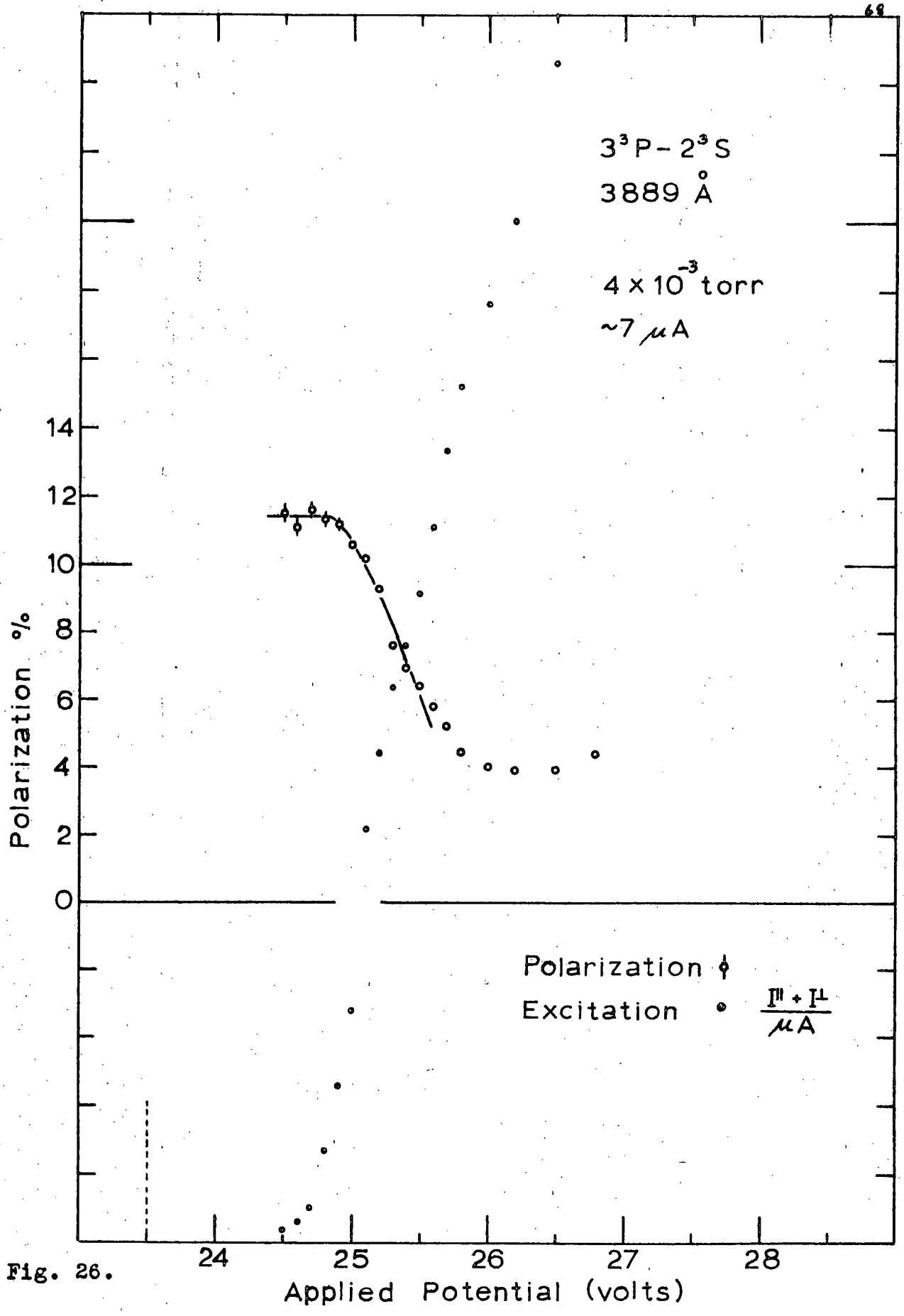
3³P - 2³S
3889 Å
4 x 10⁻³ torr
~7 μA
Polarization %
14
12
10
8
6
4
2
0
Polarization ϕ
Excitation
I∥ + I⊥ / μA
24
25
26
27
28
Applied Potential (volts)

Fig. 26.

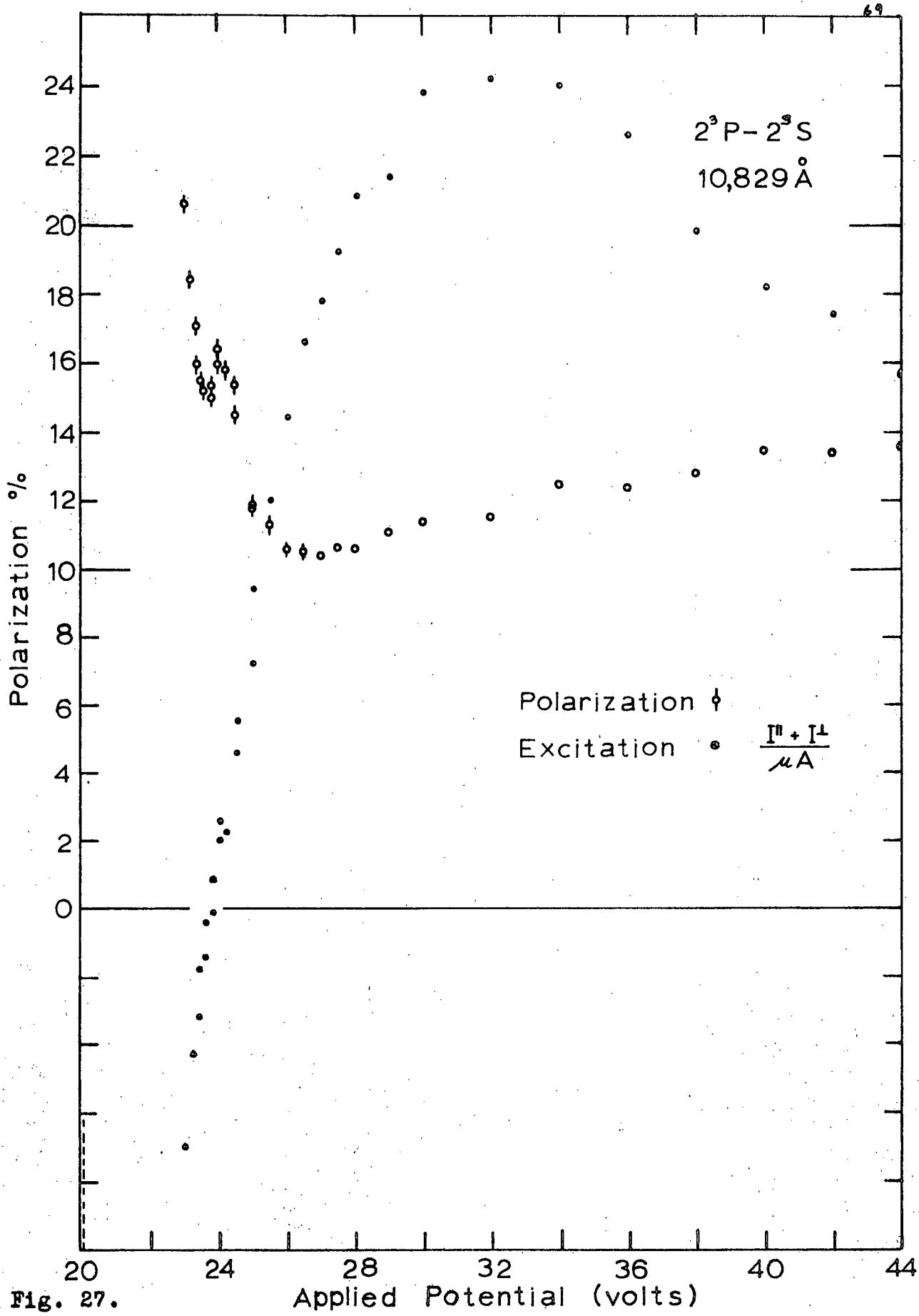
$2^3P - 2^3S$
10,829 Å
Polarization %
Polarization
Excitation
$\frac{I^{\parallel} + I^{\perp}}{\mu A}$
24
22
20
18
16
14
12
10
8
6
4
2
0
20
24
28
32
36
40
44
Applied Potential (volts)

Fig. 27.

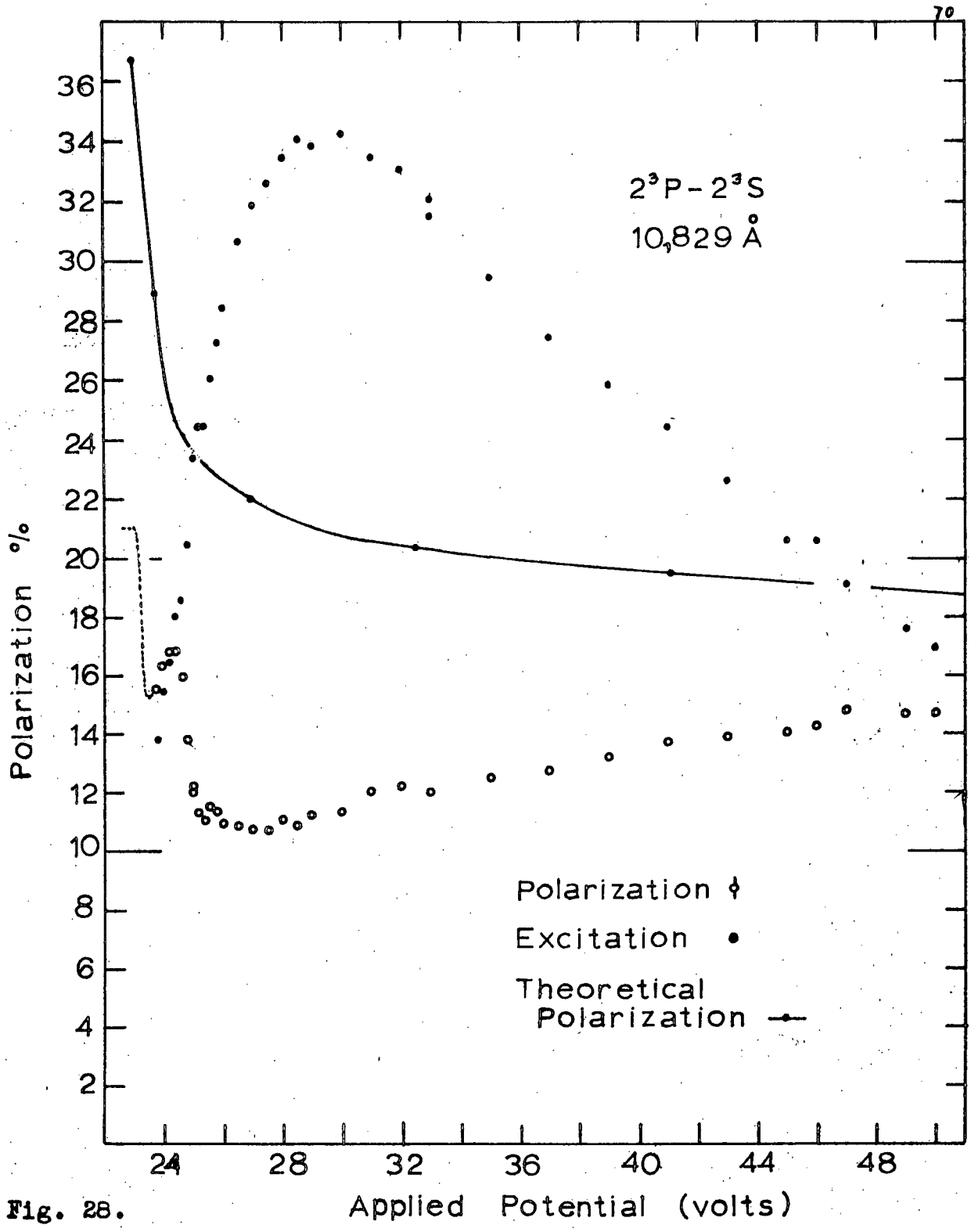
$2^3P - 2^3S$
10,829 Å
Polarization %
Applied Potential (volts)
Polarization ϕ
Excitation
Theoretical Polarization
36
34
32
30
28
26
24
22
20
18
16
14
12
10
8
6
4
2
24
28
32
36
40
44
48

Fig. 28.

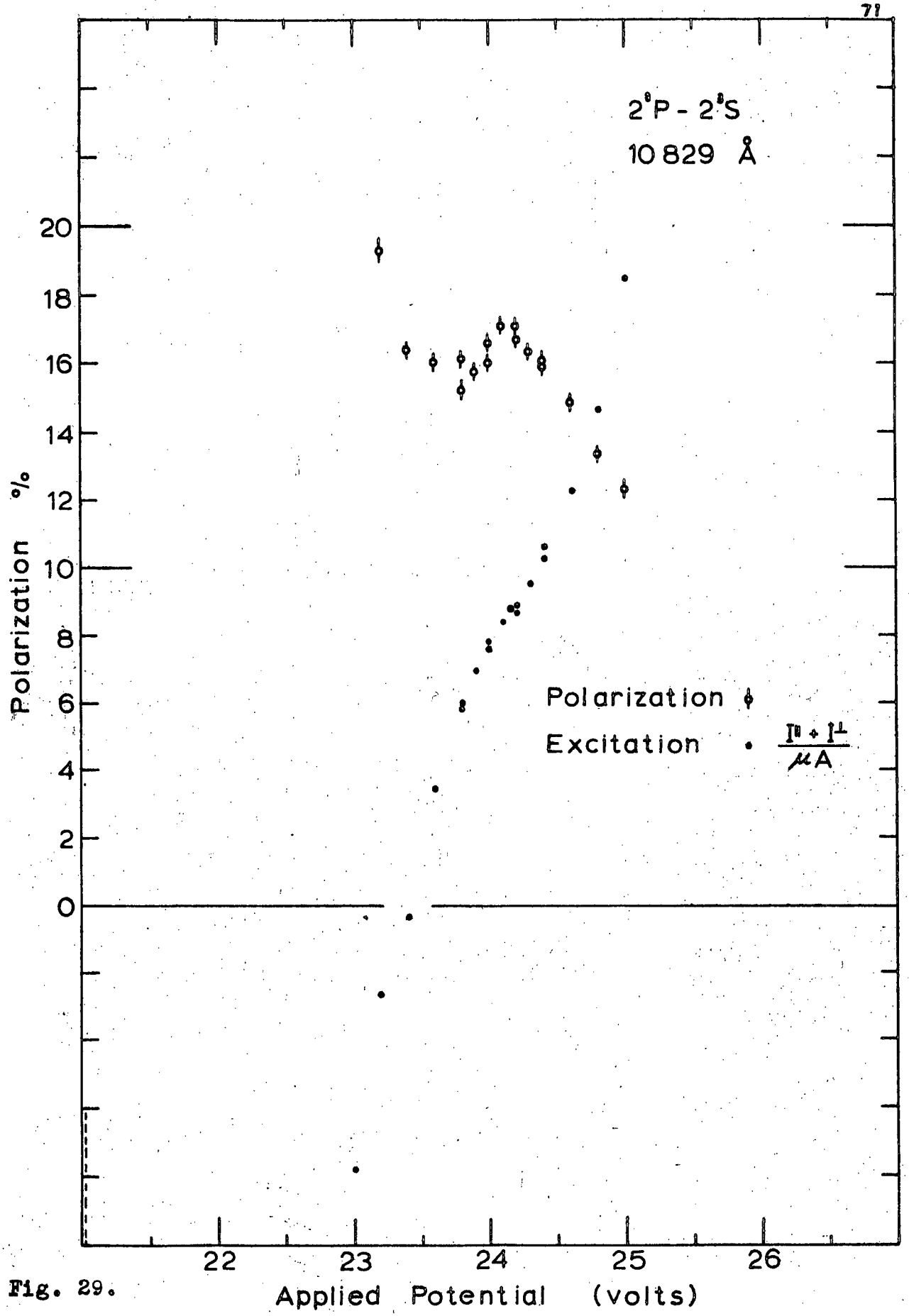
$2^3P - 2^3S$
10 829 Å
Polarization %
20
18
16
14
12
10
8
6
4
2
0
Polarization
Excitation
$\frac{I^{\parallel} + I^{\perp}}{\mu A}$
22
23
24
25
26
Applied Potential (volts)

Fig. 29.

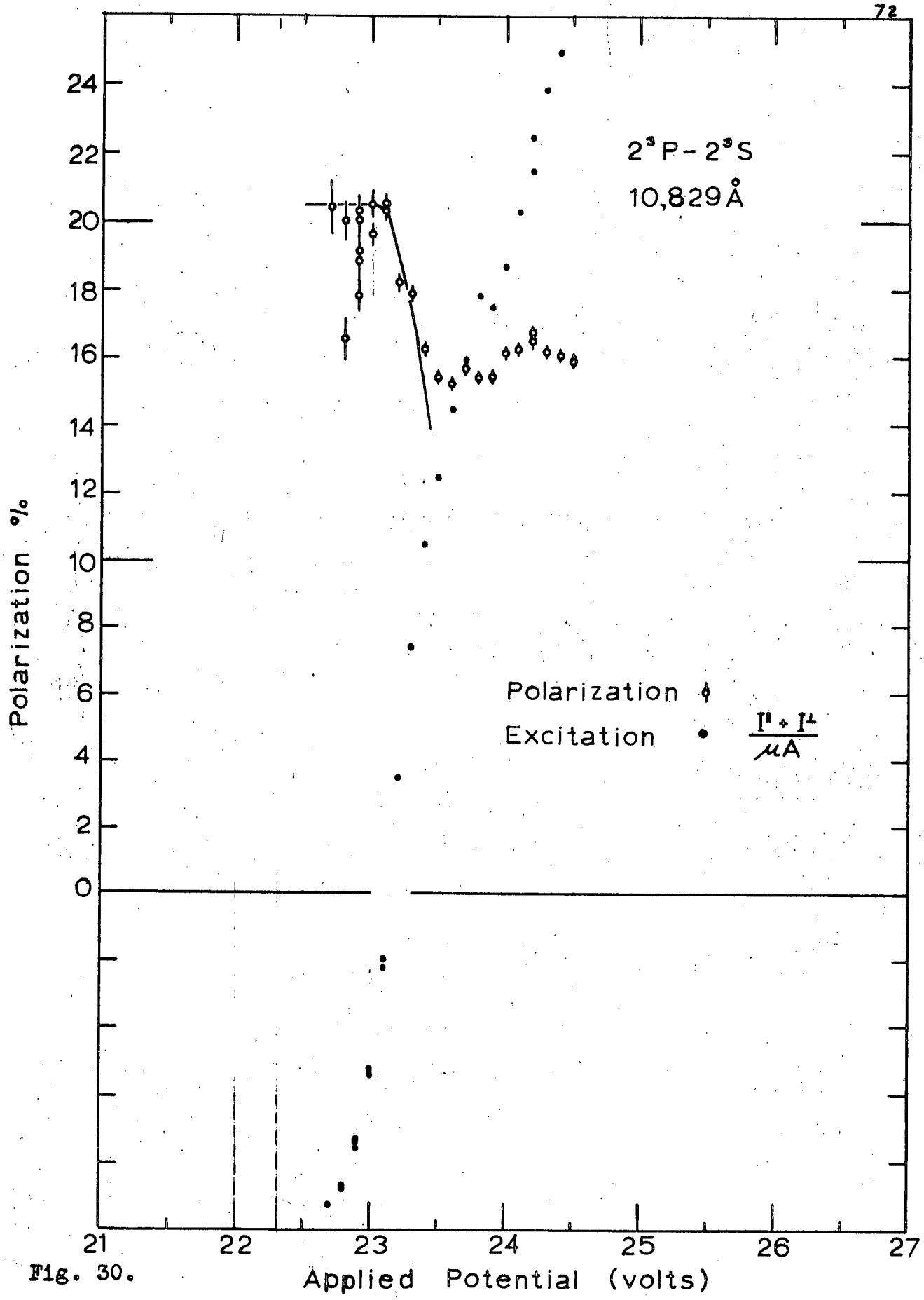
$2^3P - 2^3S$
10,829 Å
Polarization
Excitation
$\frac{I^{\parallel} + I^{\perp}}{\mu A}$
Polarization %
24
22
20
18
16
14
12
10
8
6
4
2
0
21
22
23
24
25
26
27
Applied Potential (volts)

Fig. 30.

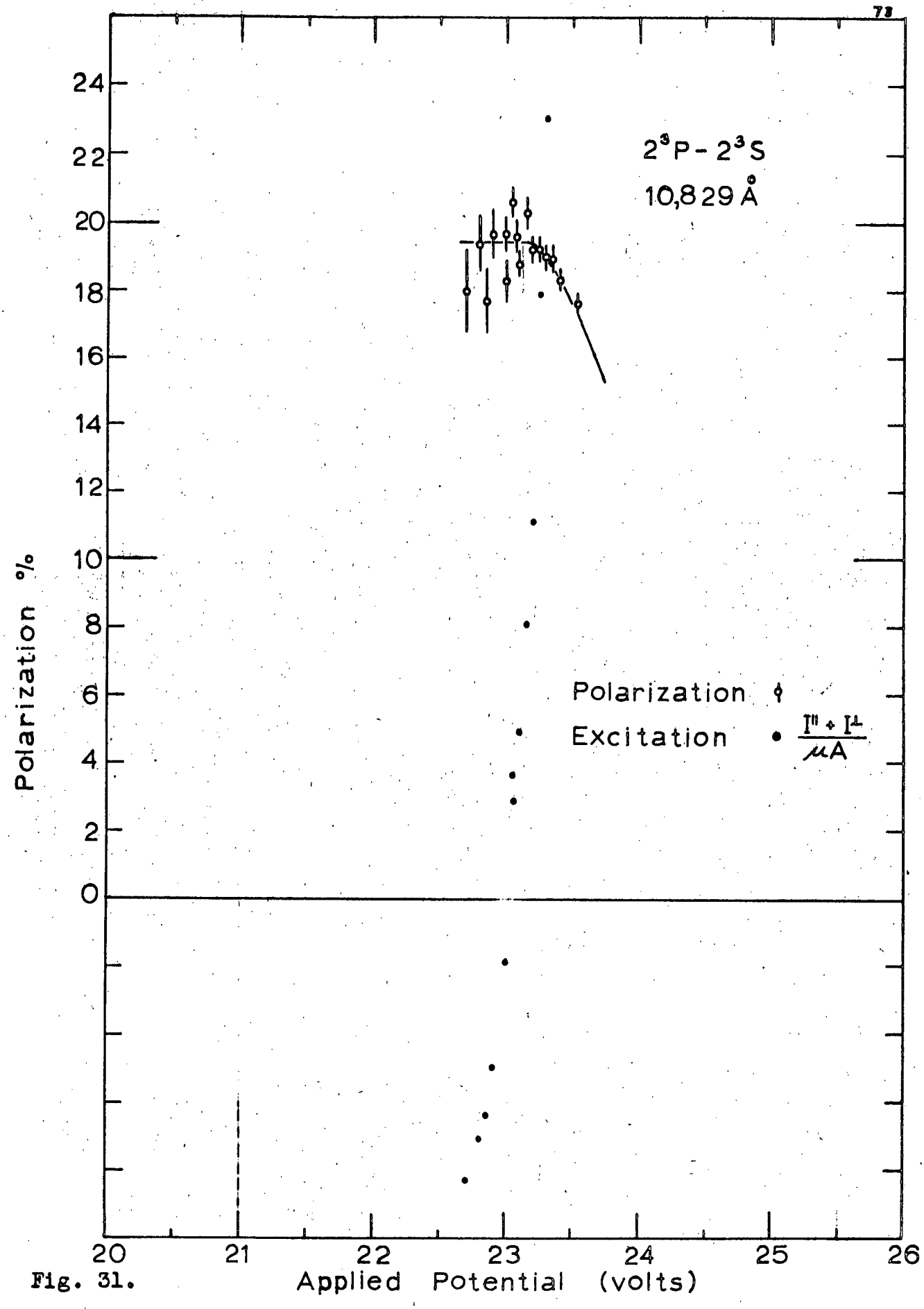
$2^3P - 2^3S$
10,829 Å
Polarization %
Polarization
Excitation
$\frac{I^{\parallel} + I^{\perp}}{\mu A}$
24
22
20
18
16
14
12
10
8
6
4
2
0
20
21
22
23
24
25
26
Applied Potential (volts)

Fig. 31.

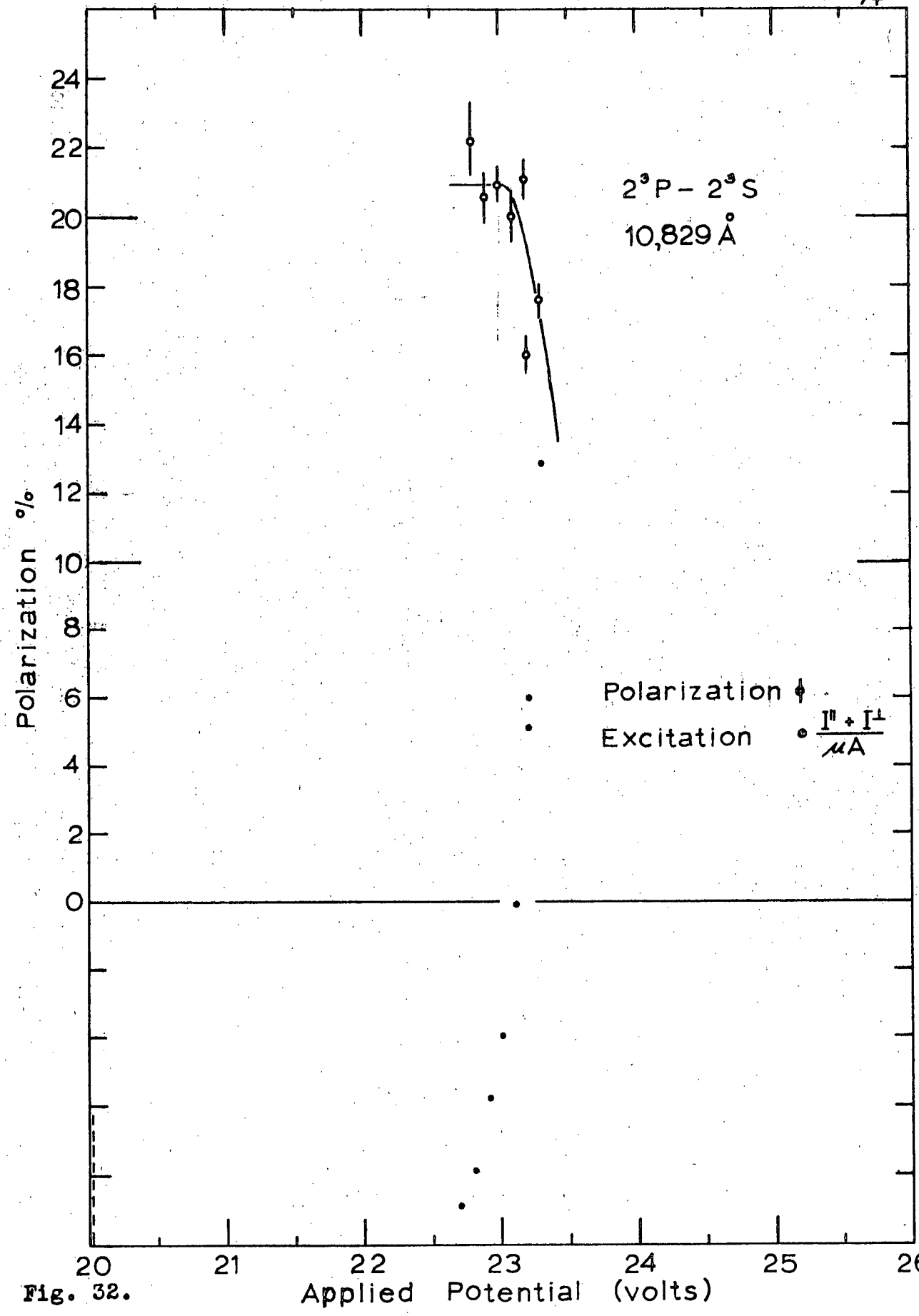
$2^3P - 2^3S$
10,829 Å
Polarization
Excitation $\frac{I^{\parallel} + I^{\perp}}{\mu A}$
Polarization %
24
22
20
18
16
14
12
10
8
6
4
2
0
20
21
22
23
24
25
26
Applied Potential (volts)

Fig. 32.

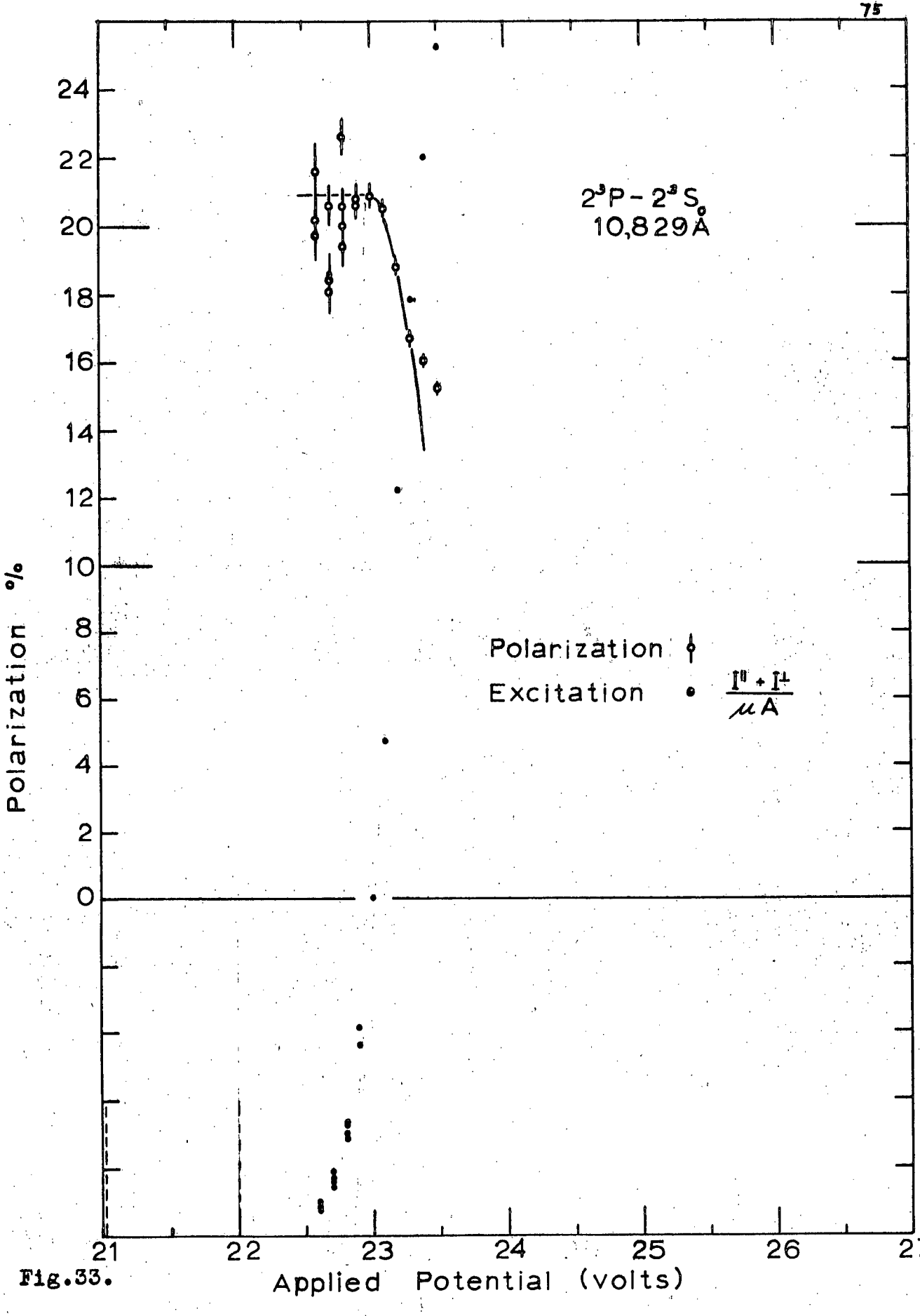
$2^3P - 2^3S$
10,829Å
Polarization
Excitation $\frac{I^{\parallel} + I^{\perp}}{\mu A}$
Polarization %
24
22
20
18
16
14
12
10
8
6
4
2
0
21
22
23
24
25
26
27
Applied Potential (volts)

Fig.33.

graphs that show the whole energy range only Figures 24 and 28 show the correct excitation curve. For the other graphs, the apparent electron beam current is an average of the "off" and "on" currents. The excitation data are expected to be less accurate than the polarization data. This is because slow drifts in signal intensity, and variations in the size of the electron beam affect the intensity data but not the polarization data. The excitation data are not considered to be accurate enough to justify polarization corrections in order to obtain relative cross sections.

The helium pressure and electron beam current are indicated on the graphs of the 3889Å line polarization. For the 10,829Å data the experimental conditions are all approximately as follows: 4×10^{-3} torr, 7μA near threshold and higher currents at higher energies. The variation of polarization with pressure is shown in Figure 34.

4.2 Energy Scale

The "applied potential" is the potential difference applied between the cathode and the scattering chamber, which was at ground potential. The thresholds for excitation are taken to be the values obtained by extrapolating the steepest parts of the intensity curves. The differences between these apparent thresholds and the

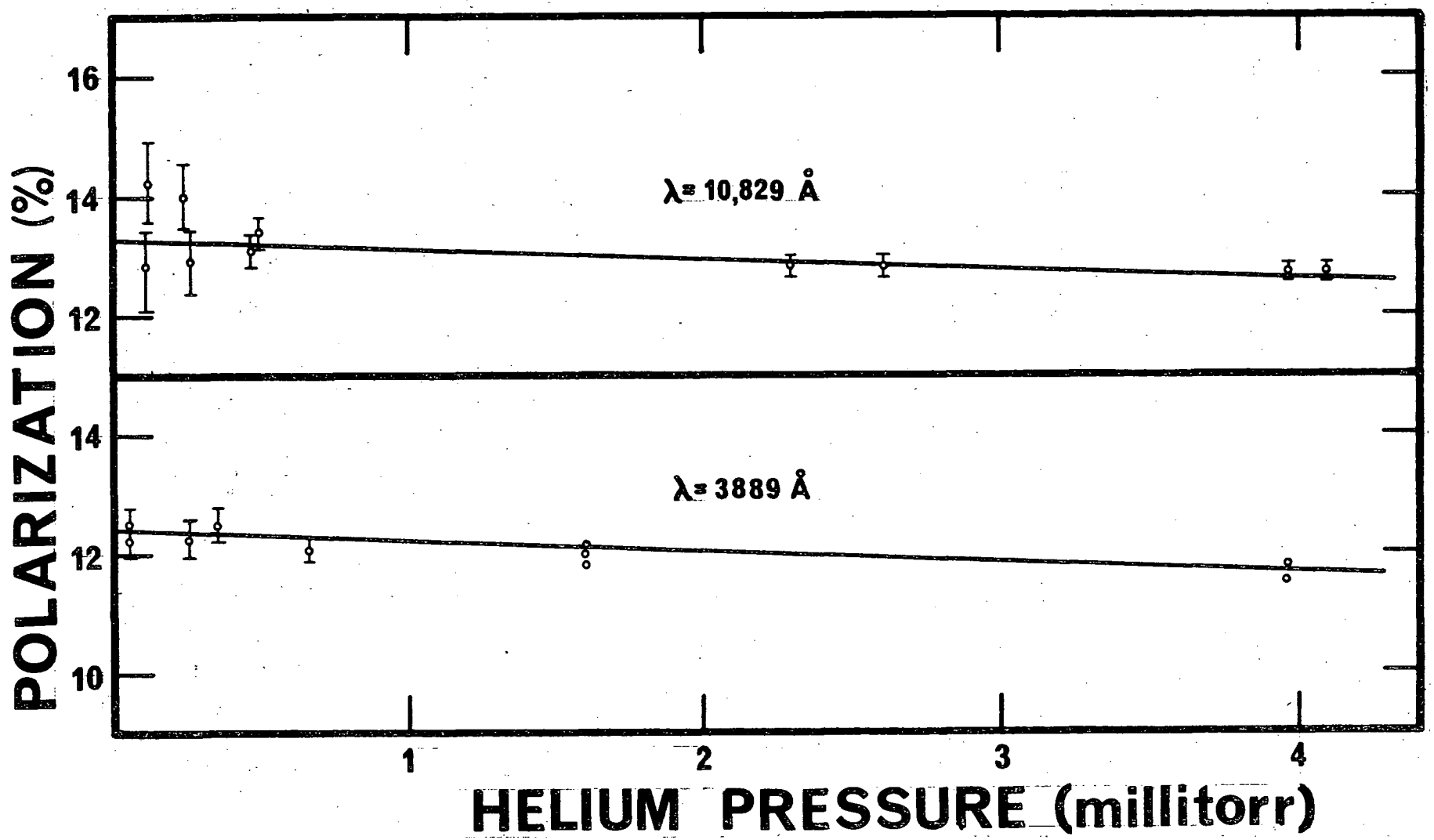

Fig. 34. Polarization as a Function of Pressure

spectroscopic values are, for the 2^3P, 3^3P, 3^3S lines respectively 1.95 volts, 1.8 volts, 1.9 volts, or 1.9 ± 0.1 volts. (Some of the curves do not show this agreement. These were taken before the voltage applied to the cathode was properly calibrated.) The threshold energies obtained from fitting curves to the polarization data tend to be a bit higher than the ones just given, but not by more than about 0.2 volts.

4.3 Experimental Sources of Error

Polarization due to optical elements. There were no elements in the optical system capable of polarizing paraxial light rays, but for the highly convergent light that was used, the mirror, the curved glass wall of the vacuum chamber, the cylindrical lens, and the interference filter can all effect the polarization. The contribution to the polarization due to the glass wall and the lens can be calculated, and are -0.5% and -0.4% respectively. (See Appendix IVA) The effects of the mirror and filter can be larger and were found by varying the aperture at the position of the lens.

In the case of the 3889Å line, the polarization as a function of aperture varied over a range of 2 or 3% (depending on the electron energy) in a way that is difficult to interpret. (See Figure 35.) At electron energies

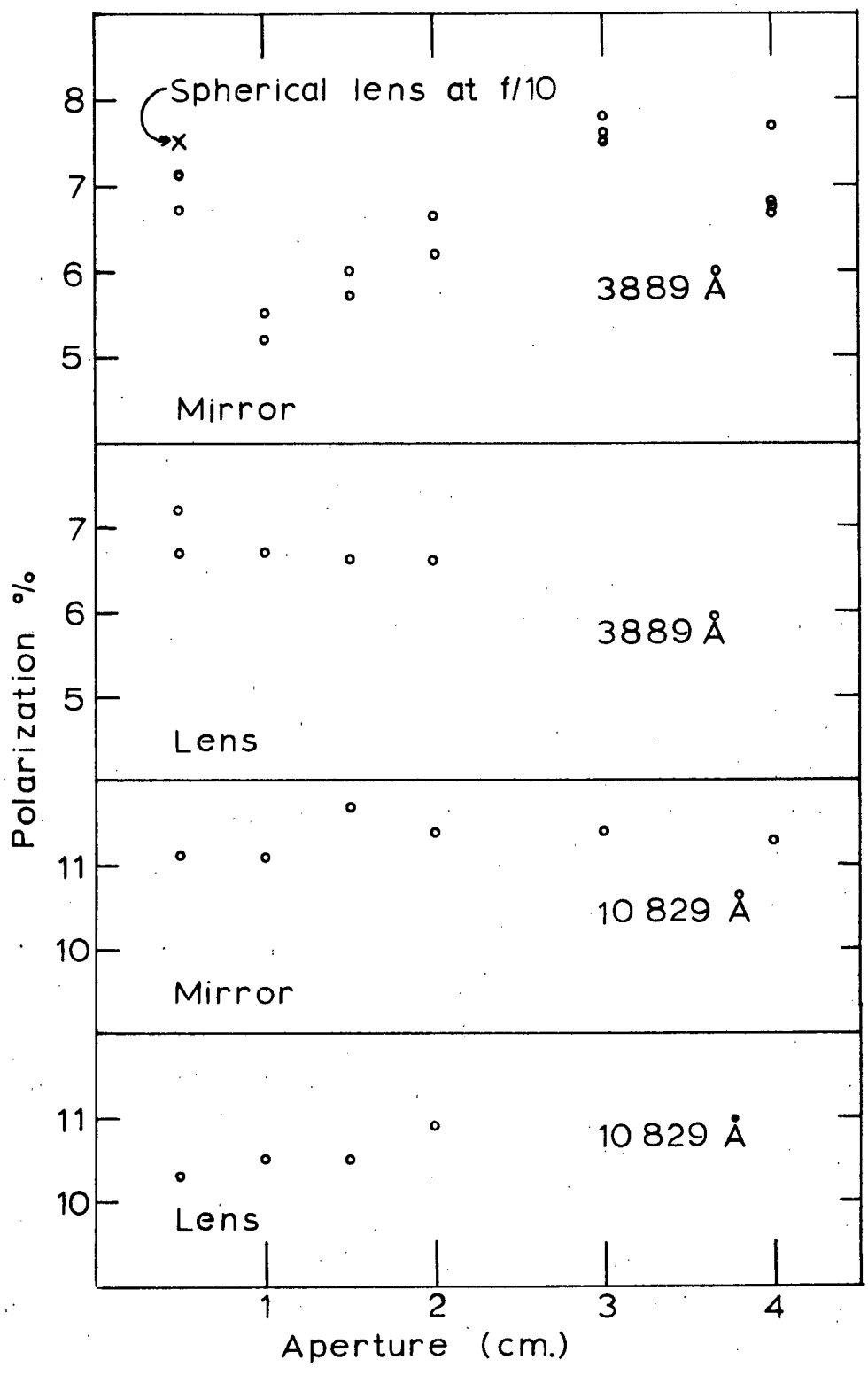

Fig. 35. Polarization as a Function of Optical Aperture.

sufficiently low that the 3889Å line was the only one within the bandpass of the filter that could be excited, it was found that the polarization at f/10 agreed with the full aperture value, while the value obtained with a spherical lens at f/10 was 1% higher. The 3889Å polarization must be considered uncertain to at least 1% on this account.

In the case of the 10,829Å line, these problems were evidently absent, since the observed polarization was independent of aperture to better than 1% (see Figure 35).

As a further check on the polarizing effect of the optics, the polarization of the 3^3S-2^3P (7065Å) line was measured. This line originates from an upper S state, and should have zero polarization. The results are shown in Figure 36. The observed polarization is about -0.4%. The rise in polarization starting at 25 volts occurs at the threshold of the $3\,^1D$-$2\,^1P$ (6678Å) line, for which the transmission of the interference filter is 0.1 times that of the 7065Å line.

Variation of polarization with angle. The cone of light collected from the excited helium extends to 0.1 radians on either side of the direction perpendicular to the electron beam. For the polarizations that were

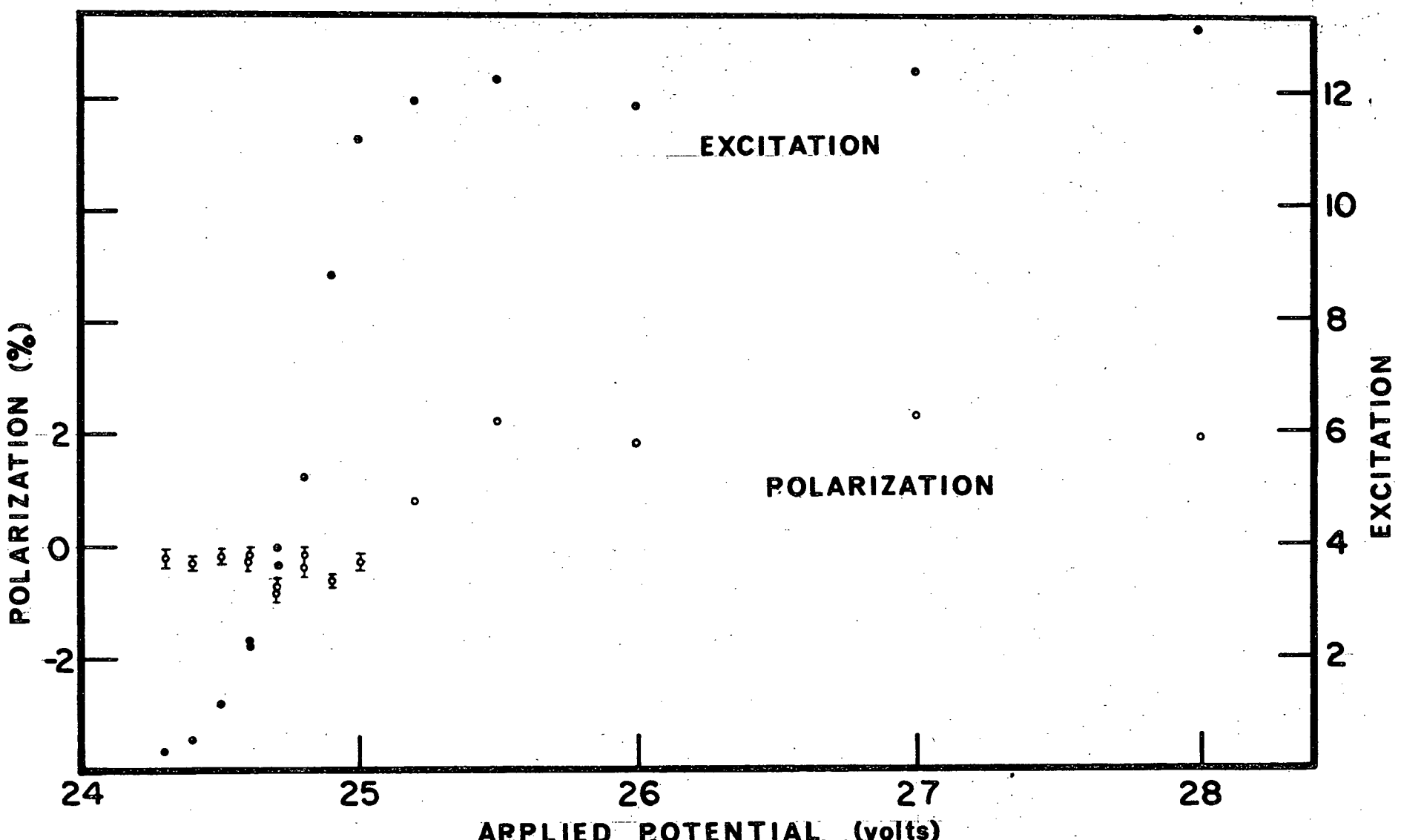

Fig. 36. Polarization and Excitation Curves for the 3^3S-2^3P (7065 A) Line

observed, this angular effect reduces the polarization by 0.1% (for P - 20%) at most, which is entirely negligible. (Refer to section 2.7.)

Dispersion of electron beam. When the electron beam was at its worst, the half angle of the electron cone was 0.13 radians. This results in a polarization of 20% being reduced by 0.2%, which again is negligible. (Refer to section 2.9.)

Coherent background. The coherent background consists of any unwanted signal that is coherent with the chopping of the electron beam. This signal was too small to measure directly. In order to estimate the effect of the coherent background signal, its magnitude was changed by a factor of perhaps 2 or 3. This was done by changing the "off" potential applied to the electron beam by 1 or 2 volts when the "on" potential was near threshold. At the lowest signal levels, the polarization of the 10,829Å line seemed to change by an amount comparable with the statistical error. This test was not done for the 3889Å line, although different "off" potentials were used for different runs. For the different runs, the plateau of polarization near threshold is reproducible, but the way in which the polarization falls

off below threshold is not. It is assumed that this fall in potential below threshold is due to the background signal.

Incoherent background. In observations of the 3889Å line, the incoherent background consisted of dark current and unmodulated light from impurity gases. The background light at 5×10^{-7} torr was 50 counts/sec. (i.e. 50 photoelectrons/sec.).

In observations of the 10,829Å line, the dominant background was light from the hot cathode which amounted to 800 to 1000 counts/sec.

These known background levels together with shot noise were used to determine the size of the error bars.

For comparison, the weakest signal in the infrared polarization curve is equivalent to 40 counts/sec.

Unwanted optical wavelengths. The interference filters have bandpasses wide enough to transmit light from other helium lines. (See Figures 12 and 13.) Near threshold, however, none of these lines are excited.

3889Å Filter: The width of the transmission curve is 140Å. Several unwanted helium lines are transmitted by this filter, which have thresholds of 0.7 volts or more above the 3889Å threshold. The relative intensities of these lines transmitted by the filter were measured with a

monochrometer. The fraction of the light that was due to these lines was found to be approximately 10% at 30 volts and 20% at 45 volts. The increase is due almost entirely to the $4\,^1D$-$2\,^1P$ (3964Å) line.

10,829Å Filter: The width of the transmission curve at half maximum is 125Å. The only interfering lines are weak ones among states of high principal quantum number. They begin at 3 volts above the 2^3P threshold and together contribute perhaps 1% of the light.

Cascading. Some of the light results from cascading from higher levels. Again, this does not occur near threshold. Cascading in helium has been discussed by Gabriel and Heddle.[2]

Electronics. The amplifiers and other components together are linear to within about 1%.

References and Footnotes for Chapter IV

1. H.S.W. Massey and B. L. Moiseiwitch, Proc. Roy. Soc. (London) Ser. A 258, 147 (1960).

2. A. H. Gabriel and D.W.O. Heddle, Proc. Roy. Soc. (London) Ser. A 258, 124 (1960).

CHAPTER V

DISCUSSION OF RESULTS AND CONCLUSIONS

5.1 Polarization Structure

In the 2^3P-2^3S polarization curve (Figures 28, 29, 30), there appears a bump at 1.2 volts above threshold. The bump is quite reproducible and the uncertainty in its peak relative to the apparent threshold is perhaps -0.2 volts. It is tempting to identify this structure with the resonance in forward inelastic electron scattering at 1.6 above threshold observed by Chamberlain.[1] However, because of the 0.4 volt discrepancy in energy and the fact that the structure does not appear as an increase in the parallel excitation function, the relationship between the bump and the resonance is unclear. An experiment with better energy resolution would help.

5.2 Threshold Polarization

In the case of the 2^3P-2^3S line particularly, the structure of the polarization curve near threshold is buried under the broad energy distribution of the electron beam. What follows is an attempt to estimate the threshold polarization by using a model of the electron energy distribution and the polarization and intensity curves. We assume that:

(i) The intensity I has the form I=kx where x is electron energy in electron volts relative to the threshold energy.

(ii) The true polarization P near threshold is given by $P = P_o (1-\gamma x)$ where P_o is threshold polarization.

(iii) The energy distribution of the electron beam having mean energy x_o is of the form $\exp -|x-x_o|/\sigma$.

Assumption (iii) is correct at least for the high energy edge of the energy distribution, since the apparent excitation curve below threshold is exponential. The resulting apparent polarization $P_a(x)$ is then given by

$$P_a(x)/P_o = 1-2\gamma\sigma \qquad x \leq 0$$

$$P_a(x)/P_o = 1-2\gamma\sigma - 4\gamma\sigma R(x/\sigma) \qquad x \geq 0$$

where

$$R(t) = (1-t+\tfrac{1}{2}t^2-\exp.(-t))/(\exp.(-t)+2t)$$

The derivation of this expression, and a graph of $P_a(x)$ are given in Appendix VA. There are two adjustable parameters σ and γ. σ was determined by fitting exponential curves to the excitation functions below threshold. γ was determined by fitting $-R(x/\sigma)$ curves to the polarization curves near threshold. The results are shown in Table III. The threshold polarizations obtained in this way are 32 ±6% for the 2^3P-2^3S line and 15±3% for the 3^3P-2^3S line. The error limits are somewhat

arbitrary, since they depend on the model, the accuracy of which is difficult to judge. However, it can be said that the data are consistent with the predicted threshold polarization for the 2^3P-2^3S line but not for the 3^3P-2^3S line.

TABLE III

THRESHOLD POLARIZATION AND OTHER PARAMETERS FOUND BY CURVE FITTING

Transition	$P_a(o)$ (%)	σ (volts)	γ (volts)	P_o (%)
$3^3P - 2^3S$	10.0	0.20	0.80	15.0
	11.4	0.16	0.78	15.4
average			0.79	15.2
$2^3P - 2^3S$	20.8	0.17	1.13	33.5
	19.0	0.20	0.5	24*
	21.0	0.15	1.07	32.0
	20.3	0.15	1.13	31.0
average			1.11	31.8
theoretical			0.27**	36.6

*Not included in the average

**Massey and Moiseiwitch

5.3 Excitation Curves

It was mentioned before that the measured excitation functions cannot be relied upon to be accurate because the

optical system is sensitive to changes in the shape of the electron beam. Nevertheless, the 3889Å excitation curve seems to exhibit more or less the same features as those measured by other workers.[2,3,4] It is expected, then, that the same is true of the 10,829Å excitation curve. In particular, it appears to flatten out slightly at about one volt above threshold in the same way as the cross section curve estimated by Holt and Krotkov.[5]

5.4 Conclusions

This thesis has reported the first measurement of the polarization due to electron impact of the 2^3P-2^3S multiplet in helium. The shape of the polarization curve is similar to that predicted by the distorted wave calculation of Massey and Moiseiwitch, but the observed polarization differs from the theoretical one in detail and in magnitude. Some structure in the 2^3P-2^3S polarization curve provides a likely connection between polarization measurements and electron scattering measurements.

This thesis has also reported a measurement of the polarization of the 3^3P-2^3S multiplet with better than usual statistical accuracy near threshold.

In answer to the question of whether the polarization approaches the theoretical value at threshold, it can be said that the polarization of the 2^3P-2^3S multiplet does,

within the uncertainties of the experiment, and that the polarization of the 3^3P-2^3S multiplet does not, at least not on an energy scale comparable with the energy resolution of the electron beam.

5.5 Suggestion for Further Work

The importance of this type of experiment lies in finding polarization values near threshold, and the obvious limitation of the work reported in this thesis is the lack of electron energy resolution. However, the energy resolution obtained in the present work is close to the limit imposed by the cathode temperature. I suggest therefore, that the next step for anyone wishing to pursue this line of investigation would be to build an electron energy selector of the type currently becoming popular in electron scattering experiments.[6] The use of such a device entails a severe reduction in electron beam current, and therefore in light intensity. However, in the experiment of this thesis there was more light than necessary at the wavelength 3889Å, and it should be possible to trade some of this for better energy resolution.

References and Footnotes for Chapter V

1. G. E. Chamberlain, Phys. Rev. 155, 46 (1967).

2. C. Smit, H.G.M. Heidman, J. A. Smit, Physica 29, 245 (1963).

3. A. H. Gabriel and D.W.O. Heddle, Proc. Roy. Soc. (London) Ser. A 258, 124 (1960).

4. I. P. Zapesochnyi and O. B. Shpenik, Soviet Phys. JETP (English Transl.) 23, 592 (1966).

5. H. K. Holt and R. Krotkov, Phys. Rev. 144, 82 (1966).

6. J. A. Simpson, Rev. Sci. Instr. 35, 1698 (1964).

APPENDIX III A

Properties of an Electron Beam

In this section, we calculate the effect of the space charge within the electron beam on two properties of the electron beam that are important in polarization studies. These properties are the energy distribution of the electrons and the radial dispersion of the electron beam.

(i) Potential Distribution in the Cross Section of an Electron Beam

We assume the electron beam to be a uniform circular cylinder, and we assume the current to be evenly distributed within that cylinder. We use cylindrical coordinates (z,r,ϕ). The radial electric field within the electron beam is given by

$$E(r) = \frac{q_\ell}{2\pi\epsilon_0 R^2}\, r$$

where R is the radius of the electron beam. In terms of the electron current I, we have

$$q_\ell = \frac{I}{\sqrt{2V\, e/m}}$$

where Ve is the energy of the electrons. Hence

$$E(r) = \frac{I}{\sqrt{2V\, e/m}\; 2\pi\epsilon_0 R^2}\, r$$

and the potential relative to the centre of the electron beam is

$$\mathbb{N}\,U(r) = \int_0^r E(r)\,dr = \frac{1}{\sqrt{2\,e/m}\;4\pi\epsilon_0}\;\frac{I}{\sqrt{V}}\;\frac{r^2}{k^2}$$

Numerically, this is

$$U(r) = 1.52 \times 10^{-2}\;\frac{I(\mu A)}{\sqrt{V}}\;\frac{r^2}{R^2}$$

where I is measured in μA and V is measured in volts. To give an example relevant to the experiment described in this thesis, we put V=25 volts, I=10μA. We find that the potential variation from the centre to the edge of the beam is 3×10^{-2} volts. This is entirely negligible because the energy variation of the electrons is much greater than this for other reasons.

(ii) Dispersion of Electron Beam due to Space Charge

As we have just seen, the radial electric field at the edge of the beam is given by

$$E(R) = \frac{I}{\sqrt{2V\,e/m}\;2\pi\epsilon_0 R}$$

The radial acceleration is then given by

$$a = \frac{e}{m}\,E(R) = \frac{\sqrt{e/m}}{2\pi\epsilon_0}\;\frac{I}{\sqrt{2V}\;R}$$

For small dispersions, the radial velocity becomes

$$v_r = at = a\,\frac{l}{v} = \frac{I}{4\pi\epsilon_0 V}\;\frac{l}{R}$$

where l is the length of the beam and v is the longitudinal velocity. Then the angle of dispersion (still assuming the dispersion is small) is given by

$$\theta = \frac{v_r}{v} = \frac{1}{4\pi\epsilon_0\sqrt{2\,e/m}}\;\frac{I}{V^{3/2}}\;\frac{l}{R}$$

$$= 1.52 \times 10^{-2}\;\frac{I(\mu A)}{V^{3/2}}\;\frac{l}{R}$$

For our example of V=25 volts, I=10μA, we have

$$\theta = 1.22 \times 10^{-3} \frac{l}{R}$$

Then if the beam is 4 cm. long and 0.1 cm. in radius, we have

$$\theta = 0.05$$

The increase in radius of the beam is given by

$$\Delta r = \frac{\theta l}{2} = 1\,mm.$$

When the electron beam was on its best behaviour, this is approximately the increase in radius that was actually observed.

APPENDIX III B

The Potential in a Region Electrostatically Shielded by Grids

We are interested in knowing how closely we must space the grids in order to shield the electron beam from stray electric fields. We use a simple two dimensional model of the situation in which an array of infinite parallel wire separated by distance a is used to shield a space from a uniform electric field.

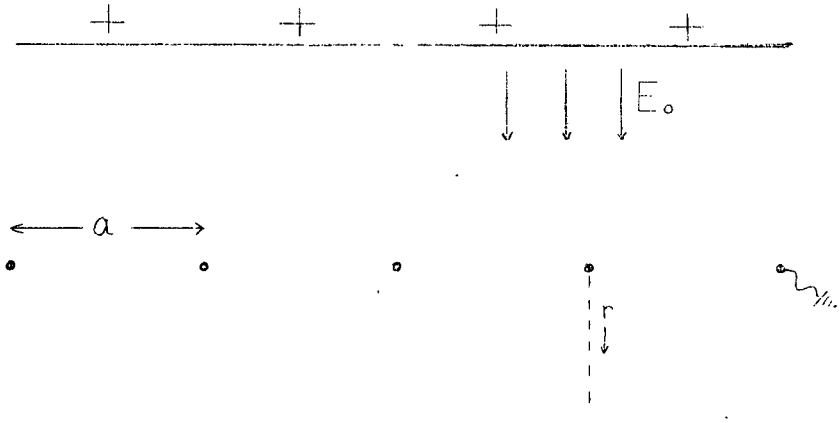

Fig. 19. Electrostatic Shield

The assumption is made that the radius r_0 of the grid wires is small compared to a.

All of the grid wires are grounded and have potential V = 0.

The average surface charge in the plane containing the grids is $E_0 \epsilon_0$, so the charge per unit length on the wires is

$$q_\ell = -E_0 \epsilon_0 a$$

Consider the electric field beneath one of the wires (along the dotted line). The field due to that wire is

$$E_1 = \frac{q\ell}{2\pi\epsilon_0 r} = -\frac{E_0}{2\pi}\frac{a}{r}$$

And the corresponding potential is

$$V_1 = \frac{E_0 a}{2\pi} \ln \frac{r}{r_0}$$

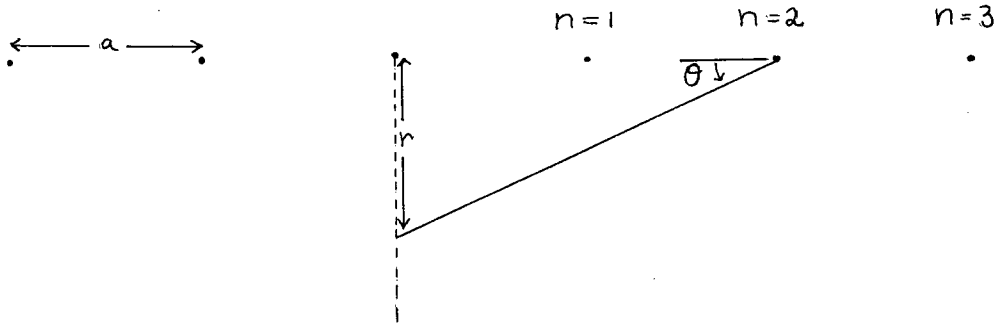

Fig. 20. Electrostatic Shield.

The field due to the remaining wires is

$$E_2 = -2\sum_{n=1}^{\infty} \frac{q\ell}{2\pi\epsilon_0} \frac{1}{\sqrt{r^2 + n^2a^2}} \sin\theta$$

$$= -2\sum_{n=1}^{\infty} \frac{q\ell}{2\pi\epsilon_0} \frac{r}{r^2 + n^2a^2}$$

$$= -\frac{E_0 a}{2\pi} \sum_{n=1}^{\infty} \frac{2r}{r^2 + n^2a^2}$$

The potential is

$$V_2 = -\int_0^2 = \frac{E_0 a}{2\pi} \sum_{n=1}^{\infty} \ln \frac{n^2a^2 + r^2}{n^2a^2}$$

$$V_2 = \frac{E_0 a}{2\pi} \ln \prod_{n=1}^{\infty} \left(1 + \frac{1}{n^2} \frac{r^2}{a^2}\right)$$

(r_o is small and is taken as zero)

The field due to the upper plate (the plane charge distribution somewhere above the grids) is

$$\frac{E_o}{2}$$

and the potential is

$$V_3 = -\frac{E_o r}{2}$$

Then the resultant potential along the dotted line is

$$V = V_1 + V_2 + V_3 = \frac{E_o a}{2\pi}\left[\ln \frac{r}{r_o} + \ln \prod - \frac{\pi r}{a}\right]$$

Introduce the dimensionless variable $x = r/a$.

Then

$$V = \frac{E_o a}{2\pi}\left[\ln \frac{a}{r_o} + \ln x + \ln \prod - \pi x\right]$$

where

$$\prod = \prod_{n=1}^{\infty} \left(1 + \frac{x^2}{n^2}\right)$$

$$= (1+x^2)\left(1+\frac{x^2}{4}\right)\left(1+\frac{x^2}{9}\right)\left(1+\frac{x^2}{16}\right)\cdots\left(1+\frac{x^2}{(N-1)^2}\right)\left[1+x^2\left(\frac{1}{N}+\frac{1}{2N^2}\right)\right]$$

where $\frac{x^2}{N} \ll 1$.

Using this method of finding $\prod$ we arrive at the values of V shown in Figure 21. We see that we are essentially in a field free region beyond one grid spacing from the grid.

At $r > a$, then, we have

$$V = \frac{E_o a}{2\pi}\left[\ln \frac{2}{r_o} - 1.84\right]$$

or, with regard to the diameter of the wire, $2r_o$, we have

$$V = \frac{E_o a}{2\pi}\left[\ln \frac{a}{2r_o} - 1.15\right]$$

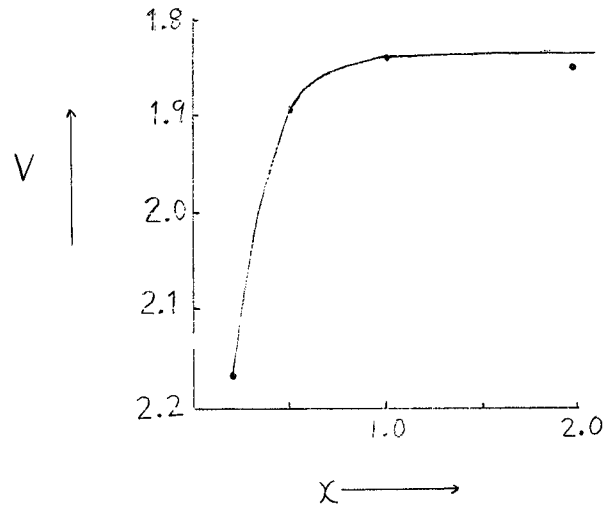

Fig. 21. Potential Inside Shield.

The practical results of these calculations are the following.

(a) In order to be free of periodic variations in potential due to the field that leaks through the spaces between the grids, we must make the grid spacing smaller than the distance between the grid and the electron beam.

(b) Provided we abide by (a), the potential in the shielded region is approximately $\Delta V = \frac{E_0 a}{2\pi}$, since the factor $\left[\ln a/2r_c - 1.15\right.$ is of order unity in practical cases. In the present experiment, we are concerned with fields of the order of 6 volts in 2 cm., or 0.3 volts per mm. The grid spacing finally used is 0.8 mm. so $\Delta V \approx \frac{0.3 \times 0.8}{2\pi} = 0.04$ volts. The fact that the shield that was used is a mesh rather than an array of wires in only

one direction should improve the shielding somewhat. We see then, that the shielding used was just about what was needed, and shielding that was very much poorer would have made a significant contribution to the electron energy spread.

APPENDIX III C

Signal Processing Theory

Transient Signals in the Output of the Lock-in Amplifier

The output signal of the phase sensitive detector is smoothed by a double section filter which is shown schematically below.

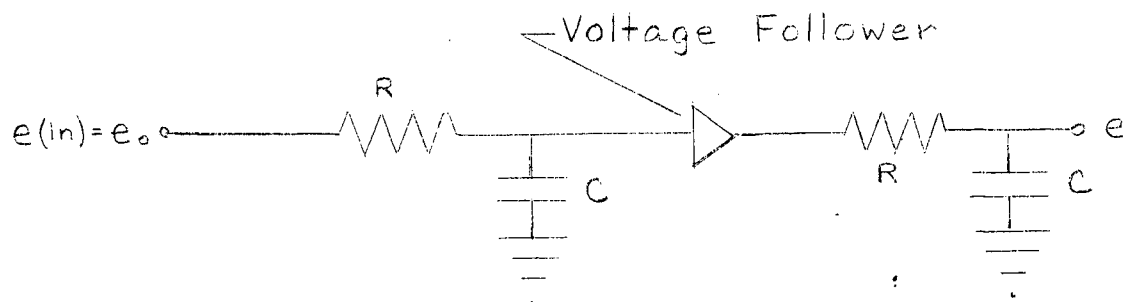

Fig. 22. RC Filter of Phase Sensitive Detector.

For polarization experiments, a time constant of RC = 1 sec. was used. The response of such a filter to a step function input voltage of the form $e(in) = e_0$ (a constant) for time $t < 0$, $e(in) = 0$ for $t > 0$ is given by

$$\frac{e}{e_0} = \left(1 + \frac{t}{RC}\right) e^{-t/RC}$$

If we put RC = 1 sec., then if we wait for 6 sec., $e/e_0 = 0.018$. The average signal during the next 14 seconds (during which time we are observing another signal) is given by e/e_0 (ave.) = 0.002. That is, the transient

signal causes an error in the next signal, (which is of a size comparable to e_c) of about 0.2%, which is small as compared with other errors.

Statistical Errors

Suppose in an observation of light intensity we count N signal pulses and N_b background pulses. The r.m.s. statistical error in the total number of counts is $\sqrt{N+N_b}$. The fractional error is then $\frac{\sqrt{N+N_b}}{N} = \frac{1}{\sqrt{N}}\sqrt{1+\frac{N_b}{N}}$.

Next we find the r.m.s. statistical error in the polarization. The factor $\sqrt{1+N_b/N}$ is independent of the direction of the observation, and we refer to it as f. The polarization is given by

$$P = \frac{N'' \pm f\sqrt{N''} - (N^{\perp} \pm f\sqrt{N^{\perp}})}{N'' + N^{\perp}}$$

The polarization is assumed to be small enough that we can ignore the error in the denominator. Thus we have

$$P = \frac{N''-N^{\perp} \pm f\sqrt{N''+N^{\perp}}}{N''+N^{\perp}} = \frac{N''-N^{\perp}}{N''+N^{\perp}} \pm \frac{f}{\sqrt{N_1+N_2}}$$

This is the formula that was used to calculate the r.m.s. errors represented by the error bars. The numbers N_1 and N_2 refer to the number of photoelectrons. The correspondence between the magnitude of the lock-in amplifier output signal and the counting rate was found by doing a run in which the signal was measured both by the usual method and by pulse counting.

Lower Limit on Useful Signal Strength

The analog to digital converter responds to positive signals only. This fact places a lower limit on the signal strength that can be used, because a sufficiently weak signal will be noisy enough that the phase sensitive detector output will be negative for part of the time. A lower limit on the signal strength implies an upper limit on useful integration times.

We now make an estimate of this upper limit under the assumption that we require r.m.s. errors of 1% or less. The output voltage x of the phase sensitive detector varies with time, and presumably the amount of time spent at each value of x is given by a gaussion distribution

$$e^{\frac{-(x-x_0)^2}{2\sigma^2}}$$

where x_0 is the average signal level. The signal will be negative 1% of the time if we choose $x_0 = 2.3\sigma$. Now the effective integration time of the double section filter is approximately 2 seconds. If we integrate the output signal from this filter over time T, the statistical uncertainty is reduced by a factor $\sqrt{2/T}$. If we now insist that this uncertainty be 1%, we require that

$$\sqrt{2/T}\,\sigma = 0.01\, x_0 = 0.01 \times 2.3\,\sigma$$

from which we find that T = 4000 seconds. In practice, integration times of about 2000 seconds were the longest used.

APPENDIX IV A

Polarization of Light due to Optical Elements

Polarization of Light due to Passage through a Glass Surface

Assume that a ray of light has an angle of incidence to the normal of a glass surface of ϕ, and an angle of refraction of ϕ'. The amplitudes of the electric fields of the transmitted light are given by

$$\frac{E_p'}{E_p} = \frac{2 \sin \phi \cos \phi}{\sin(\phi + \phi') \cos(\phi - \phi')}$$

$$\frac{E_s'}{E_s} = \frac{2 \sin \phi' \cos \phi}{\sin(\phi + \phi')}$$

(Jenkins and White, Fundamentals of Optics)

where the primes refer to refracted light and where $E_p^{(i)}$ and $E_s^{(i)}$ are the electric field components respectively parallel to, and perpendicular to the plane of incidence.

We assume the incident light to be unpolarized; i.e. $E_p^2 = E_s^2$. Then the polarization with respect to the plane of incidence of the refracted light is given by

$$P = \frac{E_p'^2 - E_s'^2}{E_p'^2 + E_s'^2} = \frac{\sin^2(\phi - \phi')}{2 - \sin^2(\phi - \phi')}$$

It is now a straightforward matter to calculate the effect on polarization of glass optical elements, especially if the angles ϕ and ϕ' are small. It is necessary to average over all the angles ϕ contained in the cone of light.

Polarization of Light due to Reflection from a Metal Surface

The situation here is somewhat more difficult than in the last section. The polarization depends on the refractive index and conductivity of the metal in a complicated way. However, for a very good reflector the effects cannot be large. An aluminum surface reflects about 90% of blue light and is somewhat better in the infrared. In general, light polarized perpendicular to the plane of incidence is reflected preferentially. This means that in the polarization experiment, any polarization due to the mirror is negative.

APPENDIX V A

Polarization Model

Consider first the intensity of light as a function of the nominal electron energy. We assume that the excitation cross section has the form

$$f(x) = kx \qquad (x \geq 0)$$
$$= 0 \qquad (x \leq 0)$$

and that the energy distribution of the electron is

$$g(x'-x) = \frac{1}{2\sigma} e^{\frac{-(x'-x)}{\sigma}}$$

where x is the nominal electron energy relative to the excitation energy, and k and σ are constants.

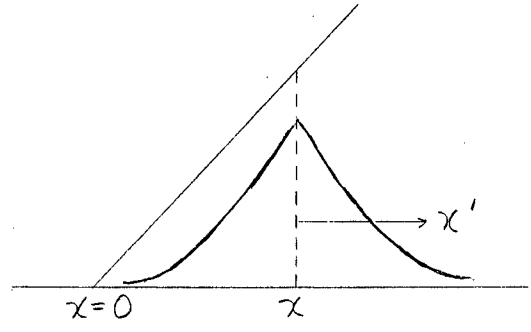

Fig. 37. Intensity Model.

Then the intensity of light is given by

$$I(x) = \int_{-\infty}^{+\infty} f(x')\, g(x'-x)\, dx'$$

Upon performing the integration, we obtain

$$I(x) = \frac{k\sigma}{2} e^{\frac{-|x|}{\sigma}} + kx \qquad (x \geq 0)$$
$$\frac{k\sigma}{2} e^{\frac{-|x|}{\sigma}} \qquad (x \leq 0)$$

Thus, below threshold, the intensity function is exponential in energy, and sufficiently far above threshold the intensity follows the excitation cross section correctly.

In order to find apparent polarization functions, we must know how to add polarizations. That is, if in a source of light there are two components with intensities I_1 and I_2, and polarizations P_1 and P_2 (referred to the same axis), the resultant polarization is

$$P = \frac{P_1 I_1 + P_2 I_2}{I_1 + I_2}$$

This may be shown easily from the definition of polarization.

It follows then, that if the polarization function is $P(x)$, the apparent polarization function $P_a(x)$ is given by

$$P_a(x) = \frac{\int_{-\infty}^{+\infty} P(x') f(x') g(x'-x)\, dx'}{\int_{-\infty}^{+\infty} f(x') g(x'-x)\, dx'}$$

The denominator is simply $I(x)$, which we have just calculated. In order to calculate the numerator, we assume the polarization function to be

$$P(x) = P_0 (1 - \gamma x) \qquad x \geq 0$$

The final result is given by

$$P_a(x)/P_0 = 1 - 2\gamma\sigma \qquad x \leq 0$$

$$P_a(x)/P_0 = 1 - 2\gamma\sigma - 4\gamma\sigma R(x/\sigma) \qquad x \geq 0$$

where

$$R(t) = \frac{1 - t^2 - \frac{1}{2}t^2 - e^{-t}}{2t + e^{-t}}$$

One apparent feature of this result is that the apparent polarization is constant below threshold. This feature is common to all such polarization models in which an exponential electron energy distribution is assumed. The reason for this is clear if it is recalled that the shape of the function $\exp.(x'-x)$, considered as a function of x', is independent of the value of x.

Another feature of this particular model is that the apparent polarization $P_a(x)$ approaches the "true" polarization $P(x)$ for large x, but more slowly than might be supposed. For $x >> \sigma$, we have

$$P_a(x) = P_0\left(1 - \gamma x - 2\frac{\gamma\sigma^2}{x}\right)$$

Graphs of the various functions are shown in Figure 38.

A convenient feature of the function $P_a(x)$ is the way in which the dependence on γ and the dependence on σ are separated in the product $4\gamma\sigma R(x/\sigma)$. This means that only one $4\gamma\sigma R(x/\sigma)$ curve has to be calculated; the others are obtained by multiplying the coordinates by appropriate factors.

The parameters σ and γ are found from the data in the following way: Exponential curves are made up on transparent sheets, and fitted to the intensity data in order to determine σ. Then $4\gamma\sigma R(x/\sigma)$ curves are made

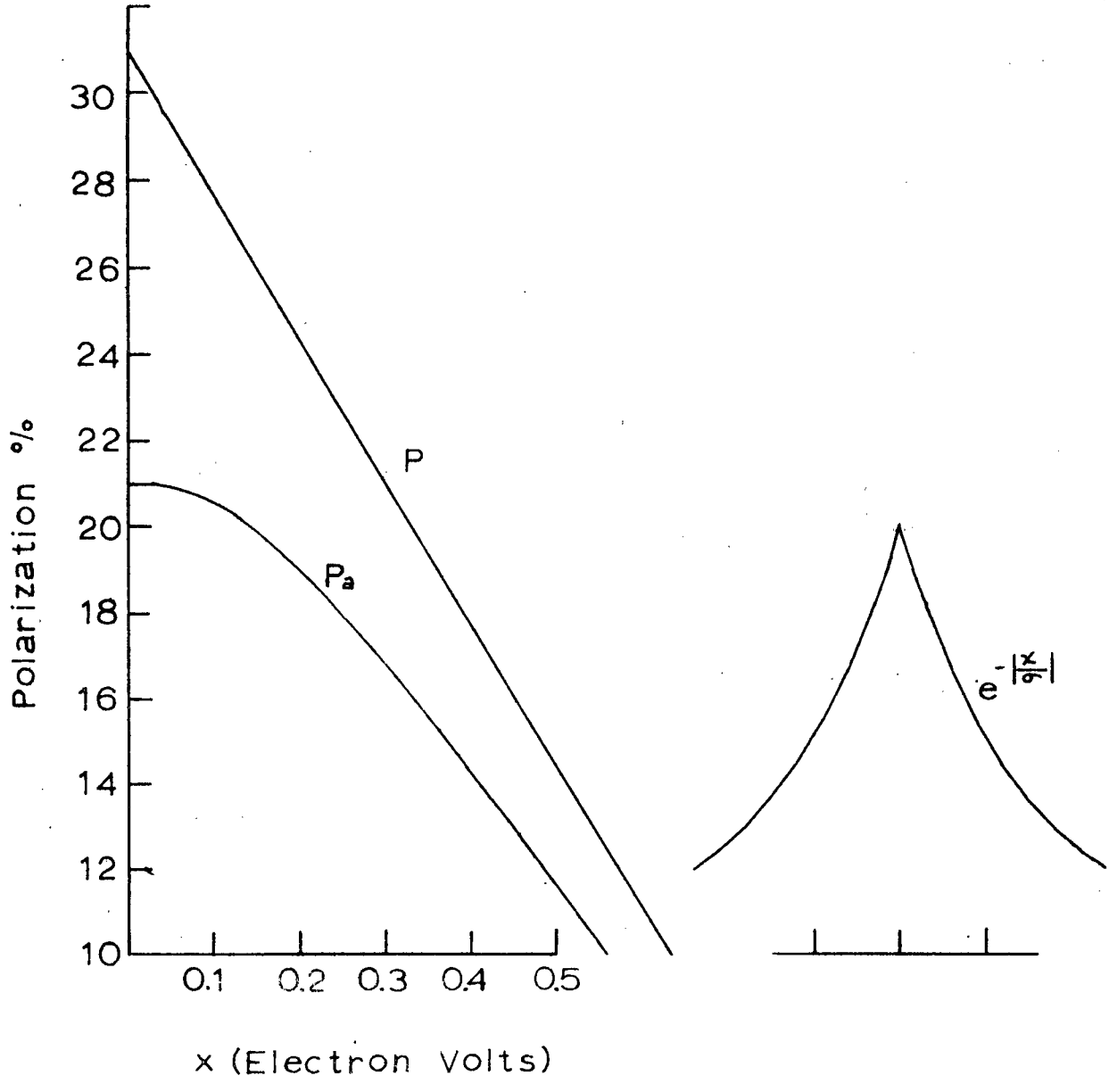

Fig. 38. Mathematical Model of Polarization.

up, for several values of $\sigma\gamma$, and fitted to the polarization data in order to determine γ. It was found necessary to make up only two sets of $4\gamma\sigma R(x/\sigma)$ curves, one for σ = 0.15 volts, and one for σ = 0.20 volts.